

Synchronization Phenomena in Coupled Hyperchaotic Oscillators with Hidden Attractors Using a Nonlinear Open Loop Controller

Ch.K. Volos, V.-T. Pham, S. Vaidyanathan, I.M. Kyprianidis
and I.N. Stouboulos

Abstract In recent years the study of dynamical systems with hidden attractors, namely systems in which their basins of attraction do not intersect with small neighborhoods of equilibria, is a great challenge due to their application in many research fields such as in mechanics, secure communication and electronics. Especially, the investigation of hyperchaotic systems with hidden attractors plays a crucial role in this research approach. Motivated by the very complex dynamical behavior of hyperchaotic systems and the unusual features of hidden attractors, a bidirectionally and unidirectionally coupling scheme of systems of this family, by using a nonlinear open loop controller, is studied in this chapter. For this reason, a recently new proposed hyperchaotic system with hidden attractors, the four-dimensional modified Lorenz system, which is structurally the simplest hyperchaotic system with hidden attractors, is used. The simulation results show that the proposed scheme drives the coupled system either to complete synchronization or anti-synchronization depending on the choice of the signs of the error function's parameters. In addition, an electronic circuit emulating the control scheme of the coupled hyperchaotic systems with hidden attractors is also presented to verify the feasibility of the proposed model.

Ch.K. Volos (✉) · I.M. Kyprianidis · I.N. Stouboulos
Physics Department, Aristotle University of Thessaloniki, GR-54124 Thessaloniki, Greece
e-mail: volos@physics.auth.gr

I.M. Kyprianidis
e-mail: imkypr@auth.gr

I.N. Stouboulos
e-mail: stouboulos@physics.auth.gr

V.-T. Pham
School of Electronics and Telecommunications, Hanoi University of Science
and Technology, 01 Dai Co Viet, Hanoi, Vietnam
e-mail: pvt3010@gmail.com

S. Vaidyanathan
Research and Development Centre, Vel Tech University,
Avadi, Chennai 600062, Tamil Nadu, India
e-mail: sundarvtu@gmail.com

Keywords Chaos · Hidden oscillation · Complete synchronization · Anti-synchronization · Bidirectional coupling · Unidirectional coupling · Nonlinear open loop controller

1 Introduction

In the last three decades the phenomenon of synchronization between coupled chaotic systems has attracted the interest of the scientific community because it is a rich and multi-disciplinary phenomenon with broad range applications, such as in secure communications [19] and cryptography [14, 60], in broadband communications systems [7] and in a variety of complex physical, chemical, and biological systems [17, 37, 41, 51, 54, 57, 62]. In general, synchronization of chaos is a process, where two or more chaotic systems adjust a given property of their motion to a common behavior, such as equal trajectories or phase locking, due to coupling or forcing. Because of the exponential divergence of the nearby trajectories of a chaotic system, having two chaotic systems being synchronized, might be a surprise. However, today the synchronization of coupled chaotic oscillators is a phenomenon well established experimentally and reasonably well understood theoretically.

The history of chaotic synchronization's theory began with the study of the interaction between coupled chaotic systems in the 1980s and early 1990s by Fujisaka and Yamada [11], Pikovsky [49], Pecora and Carroll [48]. Since then, a wide range of research activity based on synchronization of nonlinear systems has risen and a variety of synchronization's forms depending on the nature of the interacting systems and of the coupling schemes has been presented. Complete or full chaotic synchronization [9, 24–26, 28, 39, 55, 63], phase synchronization [8, 45], lag synchronization [52, 56], generalized synchronization [53], anti-synchronization [22, 36], anti-phase synchronization [1, 5, 6, 27, 58, 64], projective synchronization [38], anticipating [61] and inverse lag synchronization [34] are the most interesting types of synchronization, that have been investigated numerically and experimentally by many research groups.

This work is referred to complete synchronization and to anti-synchronization. In the first case, which is the most studied type of synchronization, two identical coupled chaotic systems leads to a perfect coincidence of their chaotic trajectories i.e., $x_1(t) = x_2(t)$ as $t \rightarrow \infty$. In the anti-synchronization, on the other hand, which is also a very interesting type of synchronization, two systems x_1 and x_2 , can be synchronized in amplitude, but with opposite sign, for initial conditions chosen from large regions in the phase space, that is $x_1(t) = -x_2(t)$ as $t \rightarrow \infty$.

As it is known, nonlinear systems and especially chaotic systems exhibit high sensitivity on initial conditions or system's parameters and thus, if they are identical and, possibly, starting from almost the same initial conditions, following trajectories which rapidly become uncorrelated. For this reason, many techniques have been set up to obtain the aim of chaotic synchronization. So, many of these techniques to couple two or more nonlinear chaotic systems can be mainly divided into two

classes: bidirectional or mutual coupling and unidirectional coupling [13]. In the mutual coupling both the systems are connected and each system's dynamic behavior influences the dynamics of the other, while on the contrary in unidirectional coupling, only the first system drives the second one.

Recently, a great interest for dynamical systems with hidden attractors has been raised. The term "*hidden attractor*" is referred to the fact that in this class of systems the attractor is not associated with an unstable equilibrium and thus often remains undiscovered because it may occur in a small region of parameter space and with a small basin of attraction in the space of initial conditions [23, 31–33, 46, 47]. In 2010, for the first time, a chaotic hidden attractor was discovered in the most well-known nonlinear circuit, in Chua's circuit, which is described by a three-dimensional dynamical system [23, 31].

The problem of analyzing hidden oscillations arose for the first time in the second part of Hilbert's 16th problem (1900) for two-dimensional polynomial systems [16]. The first nontrivial results were obtained in Bautin's works [2, 3], which were devoted to constructing nested limit cycles in quadratic systems and showed the necessity of studying hidden oscillations for solving this problem.

Later, in the middle of the 20th century, Kapranov studied [21] the qualitative behavior of Phase-Locked Loop (PLL) systems, which are used in telecommunications and computer architectures, and estimated stability domains. In that work, Kapranov assumed that in PLL systems there were self-excited oscillations only. However, in 1961, Gubar' [15] revealed a gap in Kapranov's work and showed analytically the possibility of the existence of hidden oscillations in two-dimensional system of PLL, thus, from a computational point of view, the system considered was globally stable, but, in fact, there was only a bounded domain of attraction.

Also, in the same period, the investigations of widely known Markus–Yamabe [40] and Kalman [20] conjectures on absolute stability have led to the finding of hidden oscillations in automatic control systems with a unique stable stationary point and with a nonlinearity, which belongs to the sector of linear stability [4, 10, 30].

Furthermore, systems with hidden attractors have received attention due to their practical and theoretical importance in other scientific branches, such as in mechanics (unexpected responses to perturbations in a structure like a bridge or in an airplane wing) [18, 29]. So, the study of these systems is an interesting topic of a significant importance.

In this work a hyperchaotic four-dimensional modified Lorenz system with hidden attractors, is used for studying the bidirectional or unidirectional coupling by using the nonlinear open loop controller. The simulation results from system's numerical integration as well as the circuitual implementation of the proposed system in SPICE, confirm the appearance of complete synchronization and anti-synchronization phenomena depending on the signs of the parameters of the error functions.

The chapter is organized as follows. In Sect. 2 the four-dimensional modified Lorenz system, which is used in this work, is presented. The scheme, by using the nonlinear open loop controller, in both coupling ways (bidirectional and unidirectional) as well as the simulation results are discussed in Sect. 3. Section 4 presents the circuitual implementation of the unidirectional coupling system and the simula-

tion results which are obtained by using SPICE. Finally, the conclusive remarks are drawn in the last section.

2 The Four-Dimensional Modified Lorenz System

In this work the simplest four-dimensional hyperchaotic Lorenz-type system, which has been proposed by Gao and Zhang [12], is used. This system is an extension of a modified Lorenz system, which was studied by Schrier and Maas as well as by Munmuangsaen and Srisuchinwong [42, 59]. The proposed system is described by the following set of differential equations.

$$\begin{cases} \dot{x} = y - x \\ \dot{y} = -xz + u \\ \dot{z} = xy - c \\ \dot{u} = -dy \end{cases} \quad (1)$$

It is structurally a very simple four-dimensional dynamical system having only two independent parameters (c , d). Also, as it is mentioned in [35], it has many interesting properties not found in other proposed systems, such as:

- (i) It has very few terms, only seven with two quadratic nonlinearities, and two parameters.
- (ii) All its attractors are hidden.
- (iii) It exhibits hyperchaos over a large region of parameter space.
- (iv) Its Jacobian matrix has rank less than four everywhere in the space of the parameters.
- (v) It exhibits a quasi-periodic route to chaos with an attracting torus for some choice of parameter values.
- (vi) It has regions in which the torus coexists with either a symmetric pair of strange attractors or a symmetric pair of limit cycles and other regions where three limit cycles coexist.
- (vii) The basins of attraction have an intricate fractal structure.
- (viii) There is a series of Arnold tongues [43] within the quasi-periodic region where the two fundamental oscillations mode-lock and form limit cycles of various periodicities.

All the afore-mentioned reasons make the dynamical system (1) an ideal candidate for the coupling scheme which is used in this work. Especially, the existence of hidden attractors and the hyperchaotic nature of a system like this have played a crucial role in our decision.

In this section the system's dynamic behavior is investigated numerically by employing a fourth order Runge–Kutta algorithm. For this reason, the bifurcation diagram, which is a very useful tool from nonlinear theory, is used. In Figs. 1, 2, 3, 4, 5, 6 and 7 the bifurcation diagrams of the variable y versus the parameter d , for

Fig. 1 Bifurcation diagram of y versus d for $c = 5$, with initial conditions $(x_0, y_0, z_0, u_0) = (0.55, -0.49, -0.08, 0.50)$

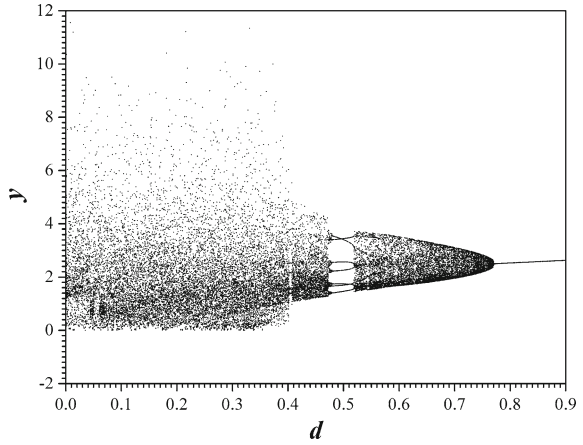


Fig. 2 Bifurcation diagram of y versus d for $c = 4$, with initial conditions $(x_0, y_0, z_0, u_0) = (0.55, -0.49, -0.08, 0.50)$

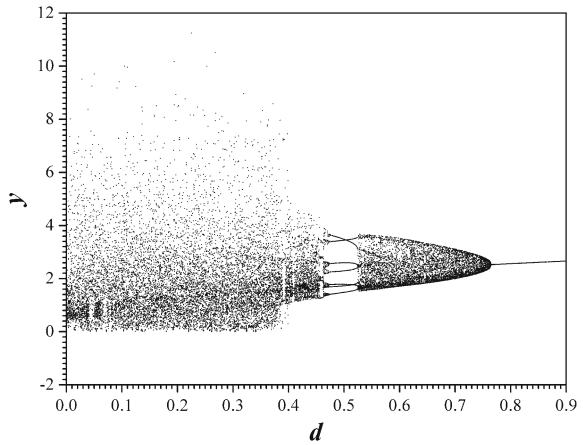


Fig. 3 Bifurcation diagram of y versus d for $c = 3.5$, with initial conditions $(x_0, y_0, z_0, u_0) = (0.55, -0.49, -0.08, 0.50)$

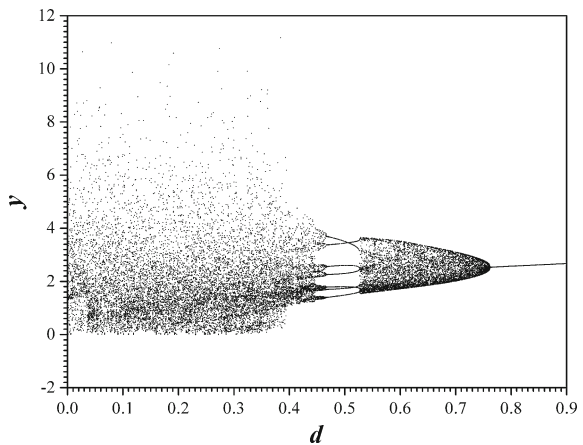


Fig. 4 Bifurcation diagram of y versus d for $c = 2.97$, with initial conditions $(x_0, y_0, z_0, u_0) = (0.55, -0.49, -0.08, 0.50)$

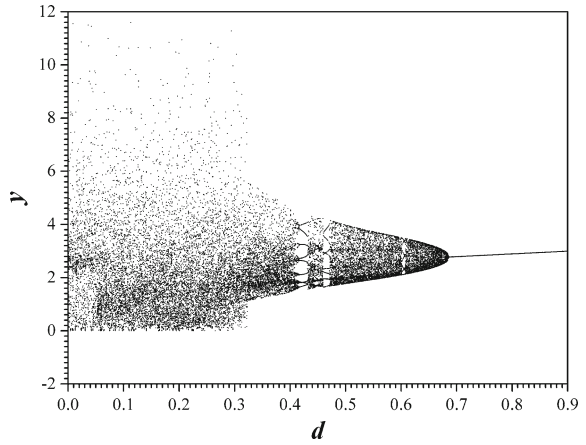


Fig. 5 Bifurcation diagram of y versus d for $c = 2.9$, with initial conditions $(x_0, y_0, z_0, u_0) = (0.55, -0.49, -0.08, 0.50)$

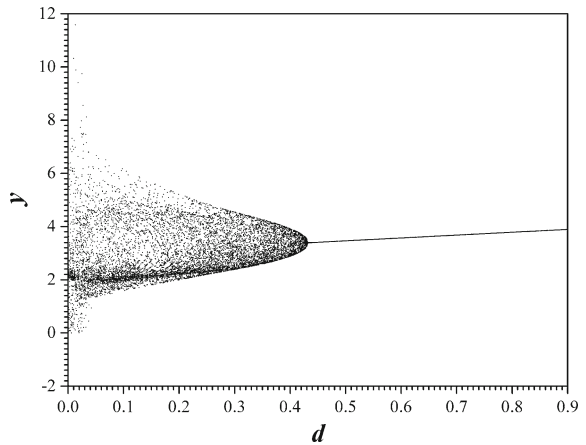


Fig. 6 Bifurcation diagram of y versus d , for $c = 2.7$, with initial conditions $(x_0, y_0, z_0, u_0) = (0.55, -0.49, -0.08, 0.50)$

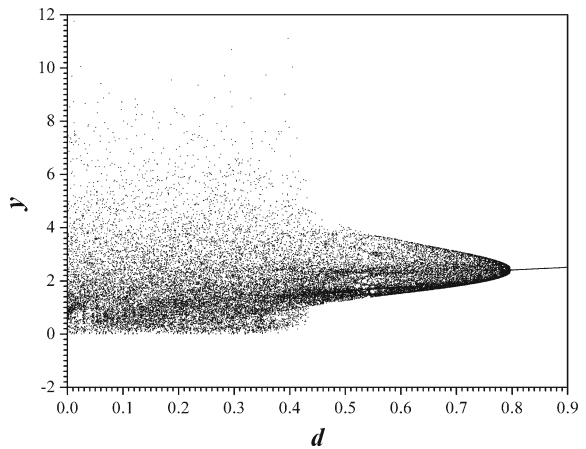
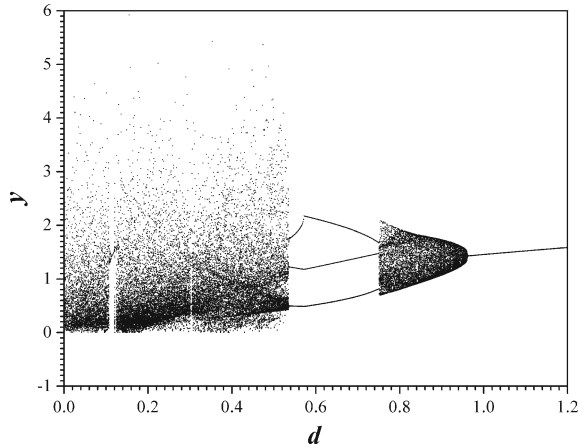


Fig. 7 Bifurcation diagram of y versus d , for $c = 1$, with initial conditions $(x_0, y_0, z_0, u_0) = (0.55, -0.49, -0.08, 0.50)$



various values of the parameter c , reveal the richness of system's dynamical behavior. Besides limit cycles, system (1) has quasi-periodicity, chaos, and hyperchaos, which can make the control of the system a difficult case in practical applications where a particular dynamic is desired. In more, details, as the value of d is decreased from $d = 0.9$ the system goes from a period-1 steady state (Fig. 8), through a quasi-periodic route (Figs. 9, 10, 11, 12 and 13), to a chaotic state, which is confirmed by the chaotic attractor in x - z plane, that is shown in Fig. 14. However, a very interesting feature of the specific system is the existence of hyperchaos for a range of parameters as it is shown in the phase portraits of Figs. 15, 16, 17, 18 and 19. Figure 20 shows

Fig. 8 Phase portrait of z versus x for $c = 2.7$ and $d = 0.9$ (period-1 state), with initial conditions $(x_0, y_0, z_0, u_0) = (0.55, -0.49, -0.08, 0.50)$

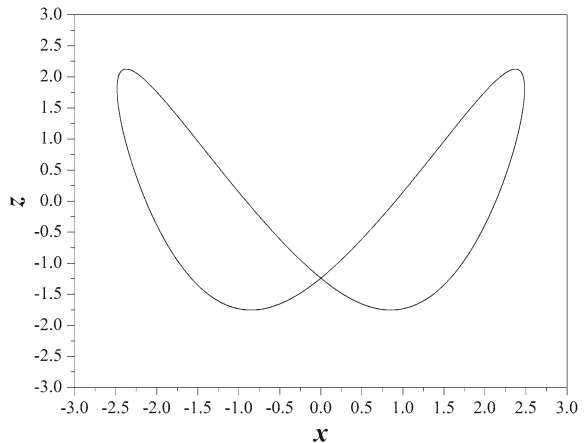


Fig. 9 Quasi-periodic attractor for $c = 2.7$ and $d = 0.75$, in x - y plane, with initial conditions $(x_0, y_0, z_0, u_0) = (0.55, -0.49, -0.08, 0.50)$

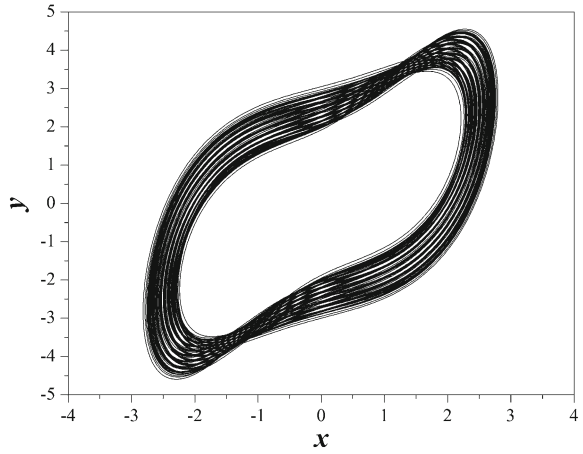


Fig. 10 Quasi-periodic attractor for $c = 2.7$ and $d = 0.75$, in x - z plane, with initial conditions $(x_0, y_0, z_0, u_0) = (0.55, -0.49, -0.08, 0.50)$

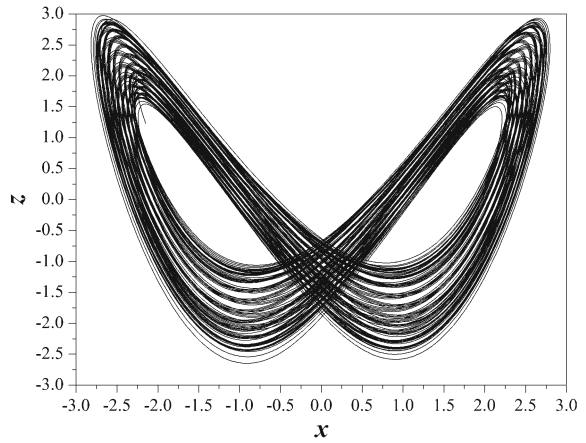


Fig. 11 Quasi-periodic attractor for $c = 2.7$ and $d = 0.75$, in x - u plane, with initial conditions $(x_0, y_0, z_0, u_0) = (0.55, -0.49, -0.08, 0.50)$

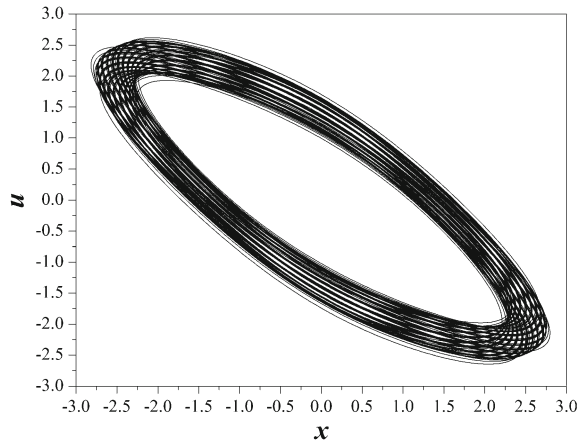


Fig. 12 Quasi-periodic attractor for $c = 2.7$ and $d = 0.75$, in y - z plane, with initial conditions $(x_0, y_0, z_0, u_0) = (0.55, -0.49, -0.08, 0.50)$

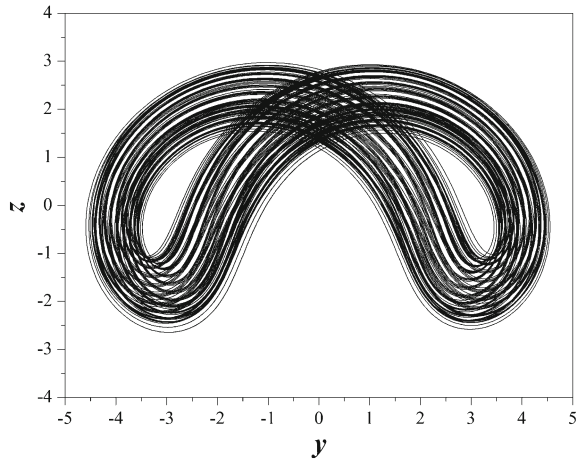


Fig. 13 Quasi-periodic attractor for $c = 2.7$ and $d = 0.75$, in y - u plane, with initial conditions $(x_0, y_0, z_0, u_0) = (0.55, -0.49, -0.08, 0.50)$

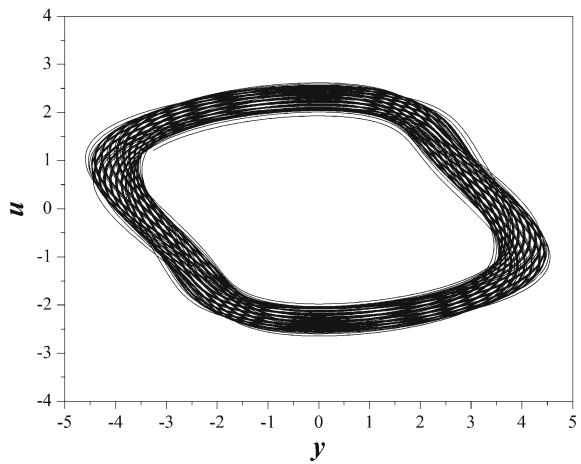


Fig. 14 Phase portrait of z versus x for $c = 2.7$ and $d = 0.2$ (chaotic state), with initial conditions $(x_0, y_0, z_0, u_0) = (0.55, -0.49, -0.08, 0.50)$

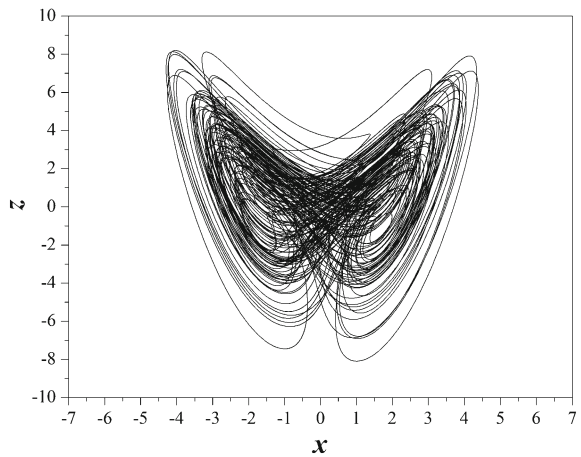


Fig. 15 Hyperchaotic attractor for $c = 2.7$ and $d = 0.44$, in x - y plane, with initial conditions $(x_0, y_0, z_0, u_0) = (0.55, -0.49, -0.08, 0.50)$

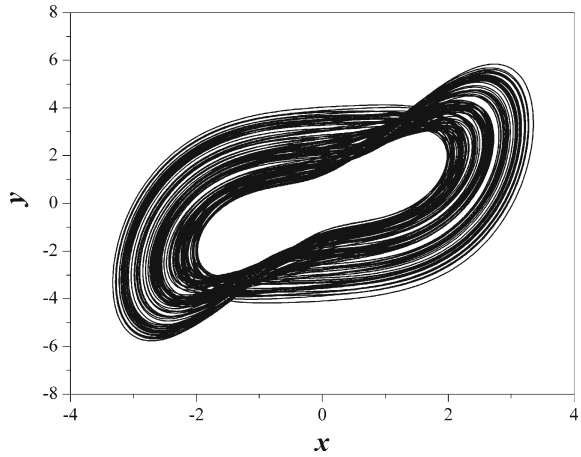


Fig. 16 Hyperchaotic attractor for $c = 2.7$ and $d = 0.44$, in x - z plane, with initial conditions $(x_0, y_0, z_0, u_0) = (0.55, -0.49, -0.08, 0.50)$

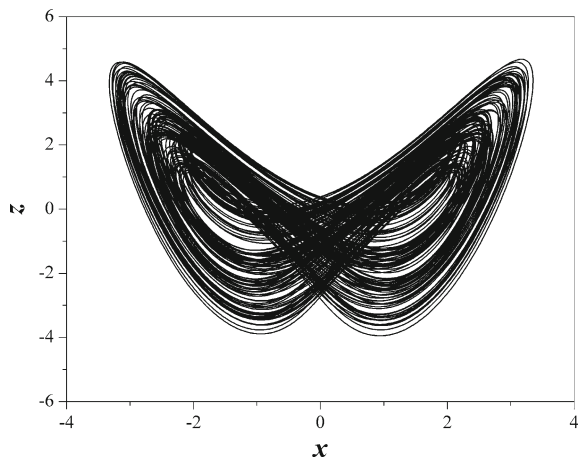


Fig. 17 Hyperchaotic attractor for $c = 2.7$ and $d = 0.44$, in x - u plane, with initial conditions $(x_0, y_0, z_0, u_0) = (0.55, -0.49, -0.08, 0.50)$

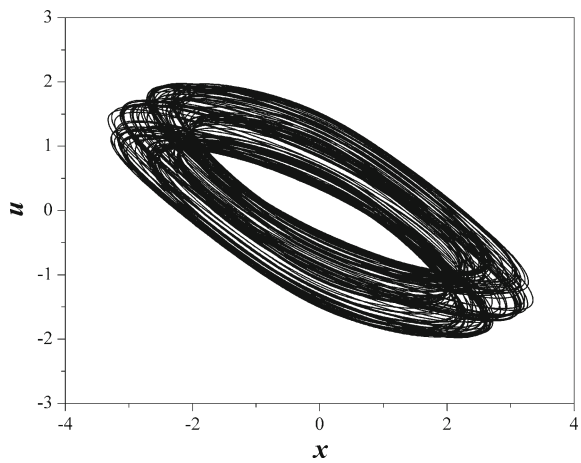


Fig. 18 Hyperchaotic attractor for $c = 2.7$ and $d = 0.44$, in y - z plane, with initial conditions $(x_0, y_0, z_0, u_0) = (0.55, -0.49, -0.08, 0.50)$

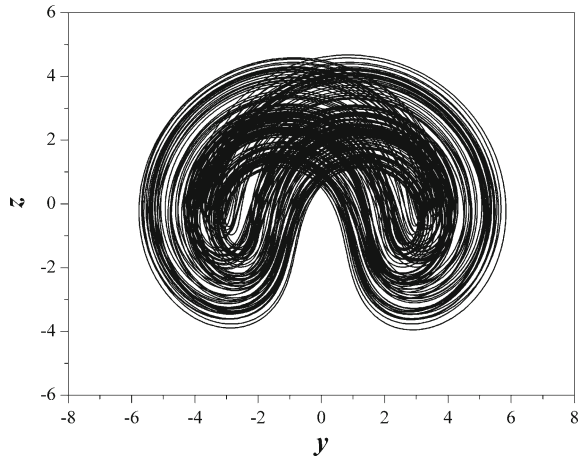
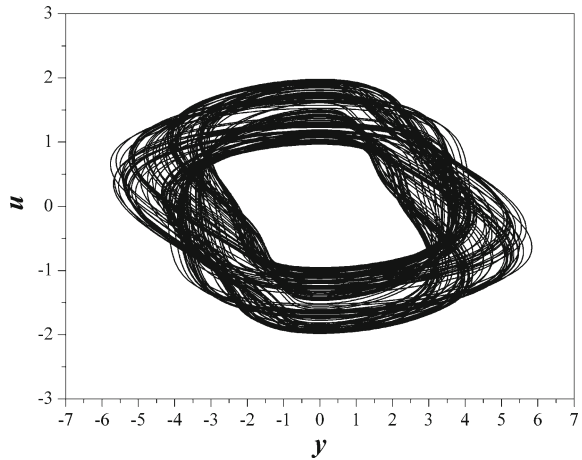


Fig. 19 Hyperchaotic attractor for $c = 2.7$ and $d = 0.44$, in y - u plane, with initial conditions $(x_0, y_0, z_0, u_0) = (0.55, -0.49, -0.08, 0.50)$



the Lyapunov exponents' spectra for chosen value of the parameter c ($c = 2.7$). The system's hyperchaotic behavior is found for $c = 2.7$ in the range of $d \in [0.388, 0.49]$ (Figs. 15, 16, 17, 18 and 19), where the system has two positive Lyapunov exponents, as it is shown in the embedded diagram in Fig. 20.

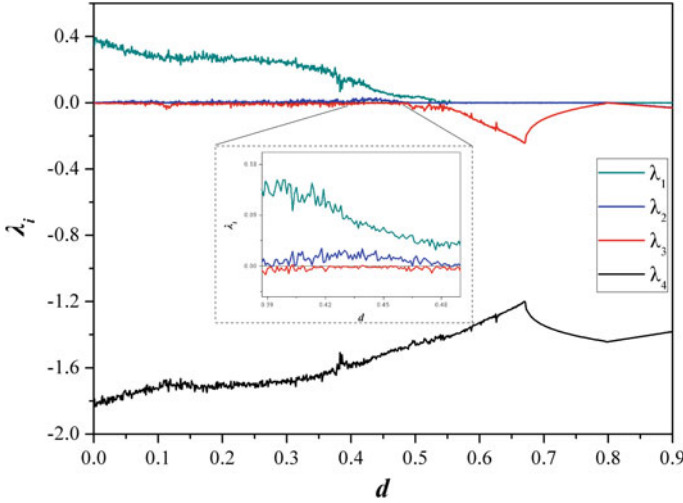


Fig. 20 The diagrams of Lyapunov exponents (λ_i) versus the parameter d , for $c = 2.7$

3 The Coupling Scheme

Two identical coupled chaotic systems can be described by the following system of differential equations:

$$\begin{cases} \dot{x} = f(x) + U_X \\ \dot{y} = f(y) + U_Y \end{cases} \quad (2)$$

where $(f(x), f(y)) \in R^n$ are the flows of the systems. The coupling of the systems is defined by the Nonlinear Open Loop Controllers (NOLCs), U_X and U_Y [44]. The error function is given by $e = \beta y - \alpha x$, where α and β are constants. If one applies the Lyapunov Function Stability (LFS) technique, a stable synchronization state will be realized when the error function of the coupled system follows the limit

$$\lim_{t \rightarrow \infty} ||e(t)|| \rightarrow 0 \quad (3)$$

so that $\alpha x = \beta y$.

As it is mentioned, the design process of the coupling scheme, is based on the Lyapunov function

$$V(e) = \frac{1}{2} e^T e \quad (4)$$

where T denotes transpose of a matrix and $V(e)$ is a positive definite function. For known system's parameters and with the appropriate choice of the controllers U_X and U_Y , the coupled system has $\dot{V}(e) < 0$. This ensures the asymptotic global stability of synchronization and thereby realizes any desired synchronization state.

By using the appropriate NOLCs functions U_X, U_Y and error function's parameters α, β , a unidirectional or bidirectional (mutual) coupling scheme can be implemented. In more details, for $(U_X = 0, \beta = 1)$ or $(U_Y = 0, \alpha = 1)$, a unidirectional coupling scheme is realized, while for $U_{X,Y} \neq 0$ and $\alpha, \beta \neq 0$, a bidirectional coupling scheme is realized, respectively. The signs of α, β play a crucial role to the type of synchronization (complete synchronization or anti-synchronization), which is observed in this work. On the other hand, the ratio of α over β decides the amplification or attenuation of one oscillator relative to another one.

Next, the results of the simulation process in the two coupling (bidirectional and unidirectional) schemes and for various values of parameters α and β are presented.

3.1 Bidirectional Coupling

Systems of chaotic oscillators bidirectionally (mutually) coupled are frequently found not only in the simulation environment or the laboratory but also in the natural world [41, 50]. This way of coupling, which is the simplest, is very interesting because it displays much of the phenomenology that is observed in more complex networks. Asymptotically stable synchronization between the coupled oscillators happens to be one of the basic phenomena that is observed.

As it is mentioned, the synchronization of coupled chaotic systems is a process where two or more systems adjust a given property of their motion to a common behavior, such as identical trajectories, due to coupling.

So, in the first case, the bidirectional coupling scheme of two coupled systems of Eq. (1), which is described by the following systems (5) and (6), is studied.

Coupled System-1:

$$\begin{cases} \dot{x}_1 = x_2 - x_1 + U_{X1} \\ \dot{x}_2 = -x_1x_3 + x_4 + U_{X2} \\ \dot{x}_3 = x_1x_2 - c + U_{X3} \\ \dot{x}_4 = -dx_2 + U_{X4} \end{cases} \quad (5)$$

Coupled System-2:

$$\begin{cases} \dot{y}_1 = y_2 - y_1 + U_{Y1} \\ \dot{y}_2 = -y_1y_3 + y_4 + U_{Y2} \\ \dot{y}_3 = y_1y_2 - c + U_{Y3} \\ \dot{y}_4 = -dy_2 + U_{Y4} \end{cases} \quad (6)$$

where $U_X = [U_{X1}, U_{X2}, U_{X3}, U_{X4}]^T$ and $U_Y = [U_{Y1}, U_{Y2}, U_{Y3}, U_{Y4}]^T$ are the NOLCs functions. The error function is defined by $\mathbf{e} = \beta \mathbf{y} - \alpha \mathbf{x}$, with $\mathbf{e} = [e_1, e_2, e_3, e_4]^T$, $\mathbf{x} = [x_1, x_2, x_3, x_4]^T$ and $\mathbf{y} = [y_1, y_2, y_3, y_4]^T$. So, the errors dynamics, by taking the difference of Eqs. (5) and (6), are written as:

$$\begin{cases} \dot{e}_1 = e_2 - e_1 + \beta U_{Y1} - \alpha U_{X1} \\ \dot{e}_2 = \alpha x_1 x_3 - \beta y_1 y_3 + e_4 + \beta U_{Y2} - \alpha U_{X2} \\ \dot{e}_3 = -\alpha x_1 x_2 + \beta y_1 y_2 - c(\beta - \alpha) + \beta U_{Y3} - \alpha U_{X3} \\ \dot{e}_4 = -de_2 + \beta U_{Y4} - \alpha U_{X4} \end{cases} \quad (7)$$

For stable synchronization $e \rightarrow 0$ as $t \rightarrow \infty$. By substituting the conditions in Eq. (7) and taking the time derivative of Lyapunov function

$$\begin{aligned} \dot{V}(e) &= e_1 \dot{e}_1 + e_2 \dot{e}_2 + e_3 \dot{e}_3 + e_4 \dot{e}_4 \\ &= e_1 (e_2 - e_1 + \beta U_{Y1} - \alpha U_{X1}) \\ &\quad + e_2 (\alpha x_1 x_3 - \beta y_1 y_3 + e_4 + \beta U_{Y2} - \alpha U_{X2}) \\ &\quad + e_3 [-\alpha x_1 x_2 + \beta y_1 y_2 - c(\beta - \alpha) + \beta U_{Y3} - \alpha U_{X3}] \\ &\quad + e_4 (-de_2 + \beta U_{Y4} - \alpha U_{X4}) \end{aligned} \quad (8)$$

we consider the following NOLC controllers:

$$\begin{cases} U_{X1} = \frac{1}{2\alpha} e_2 \\ U_{X2} = \frac{1}{\alpha} (\alpha x_1 x_3 + e_2 + e_4) \\ U_{X3} = \frac{1}{\alpha} (-\alpha x_1 x_2 + e_3) \\ U_{X4} = \frac{1}{\alpha} (-\frac{d}{2} e_2 + e_4) \end{cases} \quad (9)$$

and

$$\begin{cases} U_{Y1} = -\frac{1}{2\beta} e_2 \\ U_{Y2} = \frac{1}{\beta} (\beta y_1 y_3) \\ U_{Y3} = \frac{1}{\beta} [-\beta y_1 y_2 + c(\beta - \alpha)] \\ U_{Y4} = \frac{1}{2\beta} (de_2) \end{cases} \quad (10)$$

such that

$$\dot{V}(e) = -e_1^2 - e_2^2 - e_3^2 - e_4^2 < 0 \quad (11)$$

So, Eq. (11) ensures the asymptotic global stability of synchronization.

Next, the simulation results, in this coupling scheme, for three different cases of system's parameters (α , β), are presented.

3.1.1 The symmetric case ($\alpha = \beta$)

Firstly, the parameters α , β are chosen to be equal ($\alpha = \beta = 1$). This is the most studied type of mutual coupling and also the most interesting due to its applications in a variety of scientific fields. Also, by choosing, in this case, the systems' parameters as $c = 2.7$ and $d = 0.44$, each one of the coupled systems is in a hyperchaotic state. In this case of coupled identical systems with the proposed coupling scheme, only the complete synchronization is observed. This type of synchronization is confirmed

Fig. 21 The phase portrait of y_1 versus x_1 , for $\alpha = \beta = 1$, $c = 2.7$ and $d = 0.44$

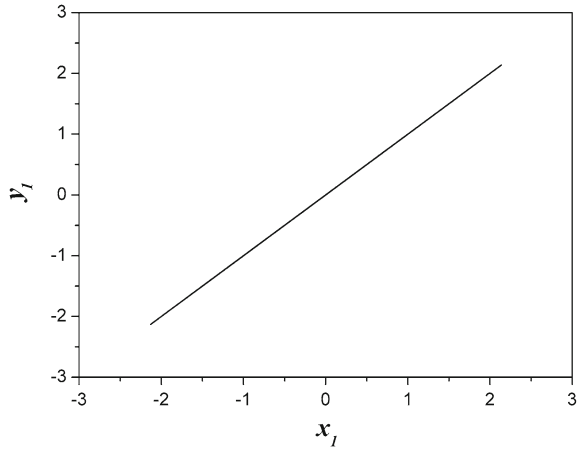
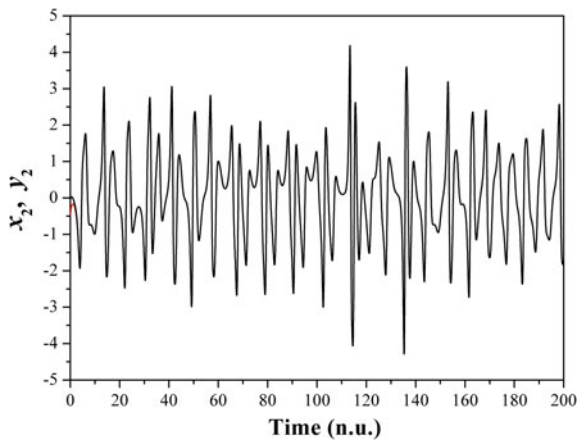


Fig. 22 The time-series of x_2, y_2 , for $\alpha = \beta = 1$, $c = 2.7$ and $d = 0.44$



by the y_1 versus x_1 plot of Fig. 21. Furthermore, the time-series of the variables x_2, y_2 as well as the errors e_i ($i = 1, 2, 3, 4$) show the exponential convergence to zero which confirms the expected system’s complete synchronization (Figs. 22 and 23).

3.1.2 The case $\alpha = 2, \beta = 1$

In this case, the parameters of the error functions are chosen to be $\alpha = 2$ and $\beta = 1$. By choosing again the systems’ parameters as $c = 2.7, d = 0.44$ and for $\alpha = 2$ the hyperchaotic attractor of the second system is enlarged by two times, as it is shown with red color in Fig. 24, as well as by the time-series of signals y_1 and y_2 in regard to the signals x_1 and x_2 respectively (Figs. 26 and 27). The y_1 versus x_1 plot in Fig. 25 confirms that the coupled system is in complete synchronization state independently

Fig. 23 The plot of errors $e_i (= \beta y_i - \alpha x_i)$, for $\alpha = \beta = 1$, $c = 2.7$ and $d = 0.44$

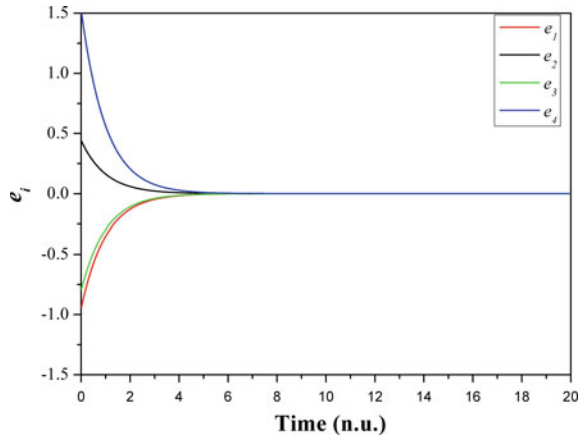


Fig. 24 The phase portraits of x_2 versus x_1 and y_2 versus y_1 , for $\alpha = 2$, $\beta = 1$, $c = 2.7$ and $d = 0.44$

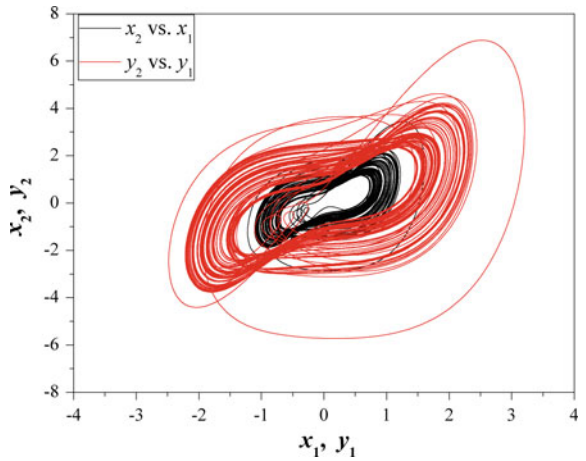


Fig. 25 The phase portrait of y_1 versus x_1 , for $\alpha = 2$, $\beta = 1$, $c = 2.7$ and $d = 0.44$

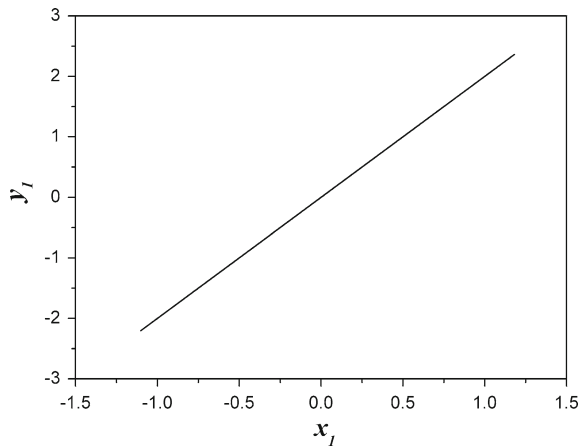


Fig. 26 The time-series of x_1, y_1 , for $\alpha = 2, \beta = 1, c = 2.7$ and $d = 0.44$

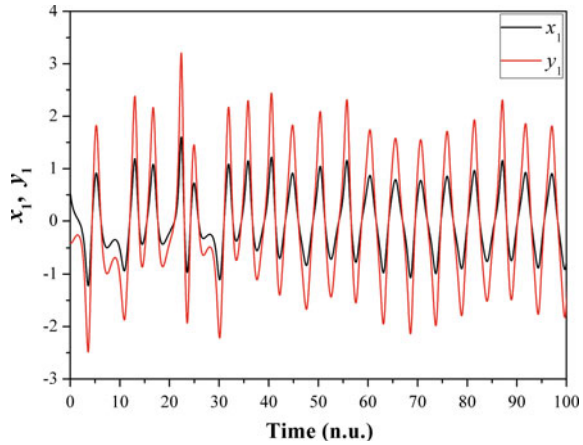
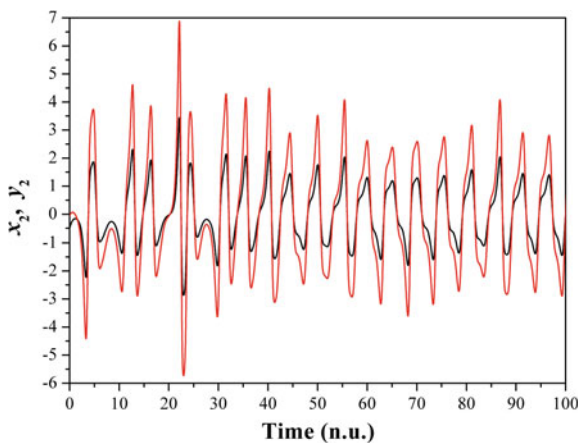


Fig. 27 The time-series of x_2, y_2 , for $\alpha = 2, \beta = 1, c = 2.7$ and $d = 0.44$



of the values of the error's parameters α, β . The error plot $e_i = y_i - 2x_i$ ($i = 1, 2, 3, 4$) in Fig. 28 shows the exponential convergence to zero that confirms the realization of system's complete synchronization state.

3.1.3 The Case $\alpha = -1, \beta = 2$

By choosing the parameters of the error functions as $\alpha = -1$ and $\beta = 2$, the attractor of the first coupled system has been enlarged by factor two, while the attractor of the second coupled system has been inverted in regard to the first one, as it is shown in Fig. 29. In this case the systems' parameters are chosen again as $c = 2.7$ and $d = 0.44$ so as both of the coupled systems are in hyperchaotic state. This process is shown more clearly in the plots of the time-series of x_1, y_1 and x_2, y_2 (Figs. 31 and 32). The phase portrait of y_1 versus x_1 in Fig. 30 indicates that the

Fig. 28 The plot of errors $e_i (= \beta y_i - \alpha x_i)$, for $\alpha = 2$, $\beta = 1$, $c = 2.7$ and $d = 0.44$

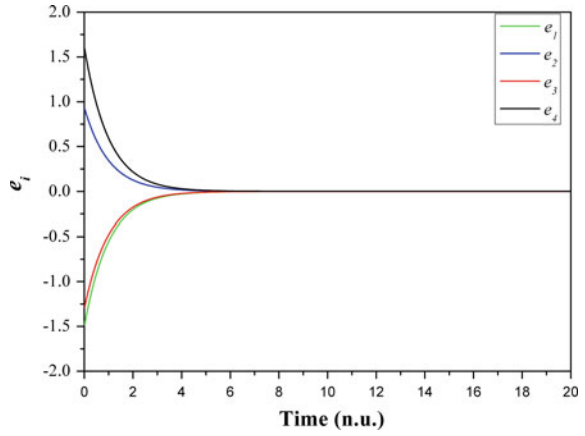


Fig. 29 The phase portraits of x_2 versus x_1 and y_2 versus y_1 , for $\alpha = -1$, $\beta = 2$, $c = 2.7$ and $d = 0.44$

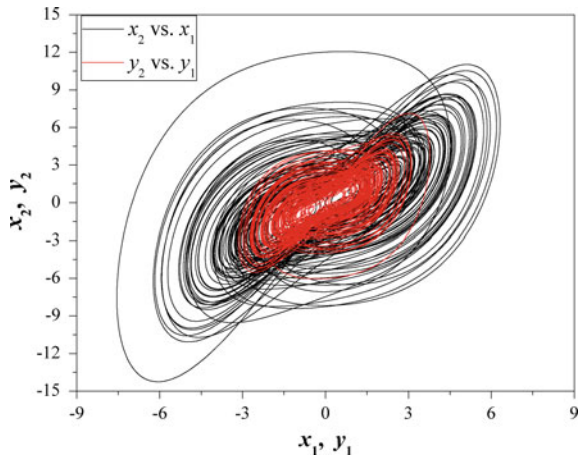


Fig. 30 The phase portrait of y_1 versus x_1 , for $\alpha = -1$, $\beta = 2$, $c = 2.7$ and $d = 0.44$

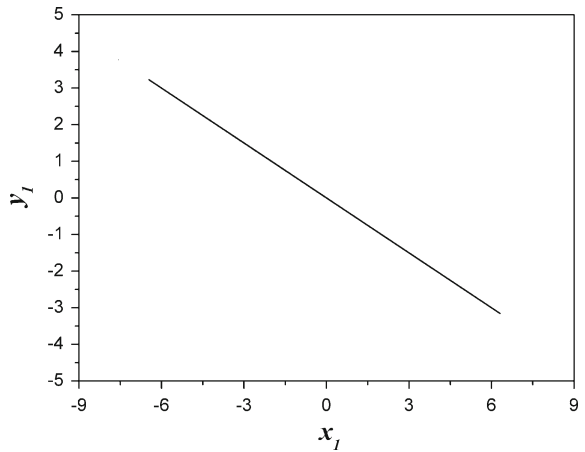


Fig. 31 The time-series of x_1, y_1 , for $\alpha = -1, \beta = 2, c = 2.7$ and $d = 0.44$

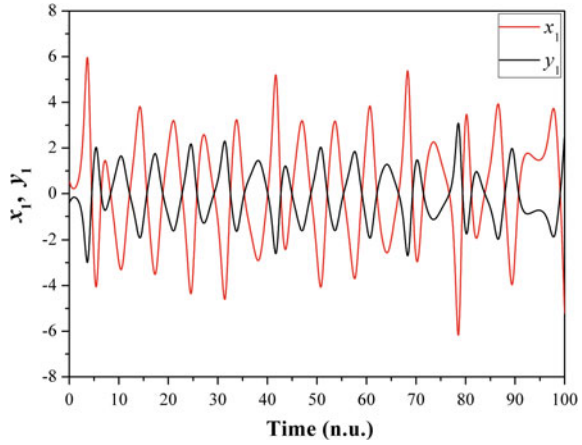
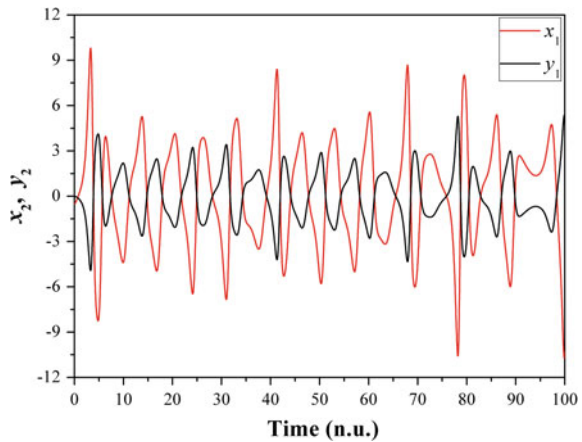


Fig. 32 The time-series of x_2, y_2 , for $\alpha = -1, \beta = 2, c = 2.7$ and $d = 0.44$



coupled system is in anti-synchronization state, which is also confirmed by the error plot $e_i = 2y_1 + x_1$ ($i = 1, 2, 3, 4$) in Fig. 33.

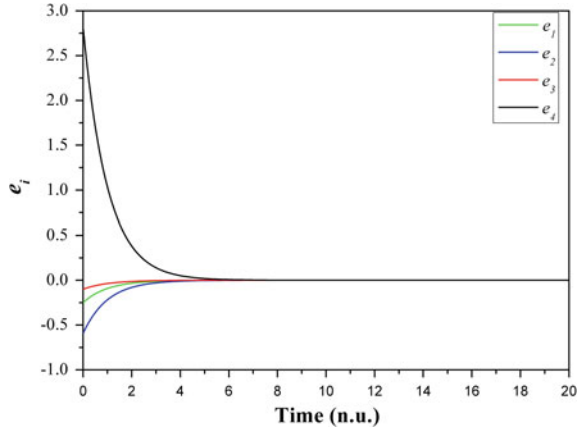
3.2 Unidirectional Coupling

In this section, the unidirectional coupling scheme, $U_X = 0$, for $\beta = 1$, given by Eq. (1), is presented.

Master System:

$$\begin{cases} \dot{x}_1 = x_2 - x_1 \\ \dot{x}_2 = -x_1x_3 + x_4 \\ \dot{x}_3 = x_1x_2 - c \\ \dot{x}_4 = -dx_2 \end{cases} \quad (12)$$

Fig. 33 The plot of errors $e_i (= \beta y_i - \alpha x_i)$, for $\alpha = -1$, $\beta = 2$, $c = 2.7$ and $d = 0.44$



Slave System:

$$\begin{cases} \dot{y}_1 = y_2 - y_1 + U_{Y1} \\ \dot{y}_2 = -y_1 y_3 + y_4 + U_{Y2} \\ \dot{y}_3 = y_1 y_2 - c + U_{Y3} \\ \dot{y}_4 = -d y_2 + U_{Y4} \end{cases} \quad (13)$$

where $U_Y = [U_{Y1}, U_{Y2}, U_{Y3}, U_{Y4}]^T$ are the Nonlinear Open Loop Controller (NOLC). The error function is defined by $e = \beta y - \alpha x$, with $e = [e_1, e_2, e_3, e_4]^T$, $x = [x_1, x_2, x_3, x_4]^T$ and $y = [y_1, y_2, y_3, y_4]^T$. So, the error dynamics, by taking the difference of Eqs. (12) and (13), are written as:

$$\begin{cases} \dot{e}_1 = e_2 - e_1 + \beta U_{Y1} \\ \dot{e}_2 = \alpha x_1 x_3 - \beta y_1 y_3 + e_4 + \beta U_{Y2} \\ \dot{e}_3 = -\alpha x_1 x_2 + \beta y_1 y_2 + c(\alpha - \beta) + \beta U_{Y3} \\ \dot{e}_4 = -d e_2 + \beta U_{Y4} \end{cases} \quad (14)$$

For stable synchronization $e \rightarrow 0$ with $t \rightarrow \infty$. By substituting the conditions in Eq. (14) and taking the time derivative of Lyapunov function

$$\begin{aligned} \dot{V}(e) &= e_1 \dot{e}_1 + e_2 \dot{e}_2 + e_3 \dot{e}_3 + e_4 \dot{e}_4 \\ &= e_1 (e_2 - e_1 + \beta U_{Y1}) + e_2 (\alpha x_1 x_3 - \beta y_1 y_3 + e_4 + \beta U_{Y2}) \\ &\quad + e_3 [-\alpha x_1 x_2 + \beta y_1 y_2 + c(\alpha - \beta) + \beta U_{Y3}] + e_4 (-d e_2 + \beta U_{Y4}) \end{aligned} \quad (15)$$

we consider the following NOLC controllers

$$\begin{cases} U_{Y1} = -\frac{1}{\beta}e_2 \\ U_{Y2} = -\frac{1}{\beta}(e_2 + \alpha x_1 x_3 - \beta y_1 y_3 + e_4) \\ U_{Y3} = -\frac{1}{\beta}[e_3 - \alpha x_1 x_2 + \beta y_1 y_2 + c(\alpha - \beta)] \\ U_{Y4} = -\frac{1}{\beta}(e_4 - de_2) \end{cases} \quad (16)$$

such that

$$\dot{V}(e) = -e_1^2 - e_2^2 - e_3^2 - e_4^2 < 0 \quad (17)$$

Equation (17) ensures the asymptotic global stability of synchronization.

3.2.1 The Case $\alpha = \beta = 1$

In this case, as it occurs in the mutual coupling, the phenomenon of complete synchronization is achieved for every value of $\alpha = \beta$. Especially, for $\alpha = \beta = 1$, the two coupled systems are in the same hyperchaotic state, due to the chosen values of system's parameters ($c = 2.7$ and $d = 0.44$). The goal of complete synchronization is achieved as it is shown from the plots of y_1 versus x_1 , the time-series of x_2, y_2 and the errors e_i in Figs. 34, 35 and 36.

3.2.2 The Case for $\alpha = -\beta = -1$

By using opposing values for the parameters $\alpha = -\beta = -1$ the phenomenon of anti-synchronization is achieved, as it is shown in Fig. 37. Initially, the coupled systems are in different hyperchaotic states but the unidirectional coupling leads the slave system to an opposite hyperchaotic attractor in regard to the master system. This conclusion is derived from the phase portrait of y_1 versus x_1 (Fig. 37), as well as from the

Fig. 34 The phase portrait of y_1 versus x_1 , for $\alpha = \beta = 1, c = 2.7$ and $d = 0.44$

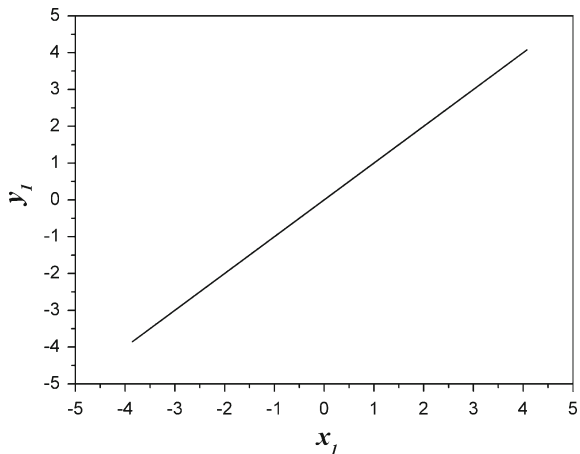


Fig. 35 The time-series of y_2, x_2 , for $\alpha = \beta = 1$, $c = 2.7$ and $d = 0.44$

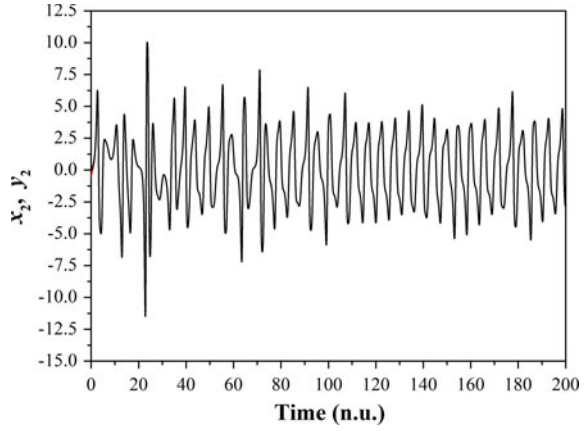


Fig. 36 The plot of errors $e_i (= \beta y_i - \alpha x_i)$, for $\alpha = \beta = 1$, $c = 2.7$ and $d = 0.44$

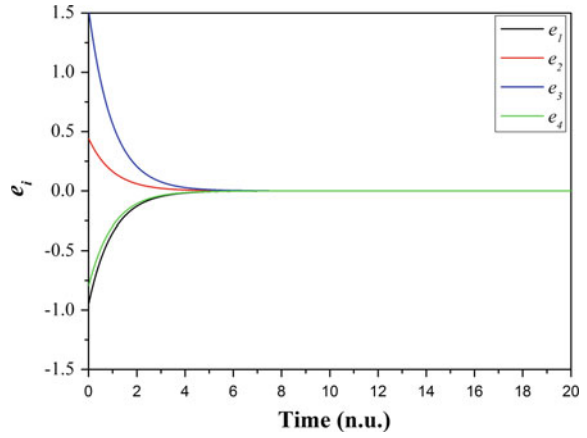


Fig. 37 The phase portrait of y_1 versus x_1 , for $\alpha = -\beta = -1$, $c = 2.7$ and $d = 0.44$

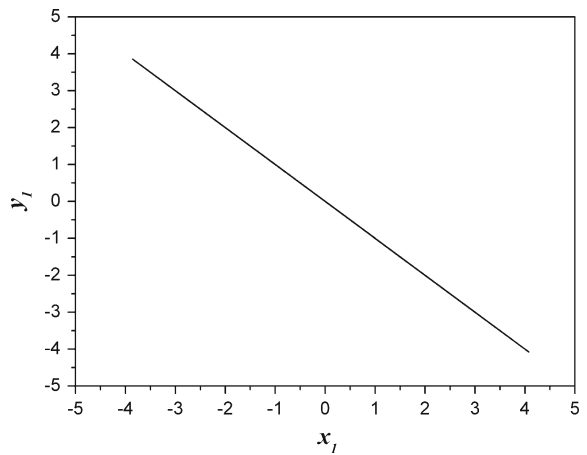


Fig. 38 The time-series of y_2, x_2 , for $\alpha = -\beta = -1$, $c = 2.7$ and $d = 0.44$

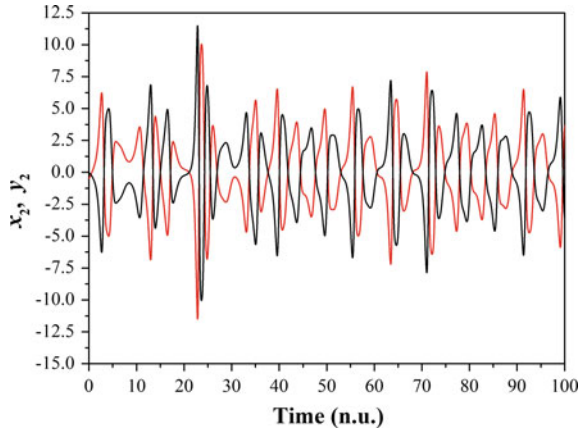
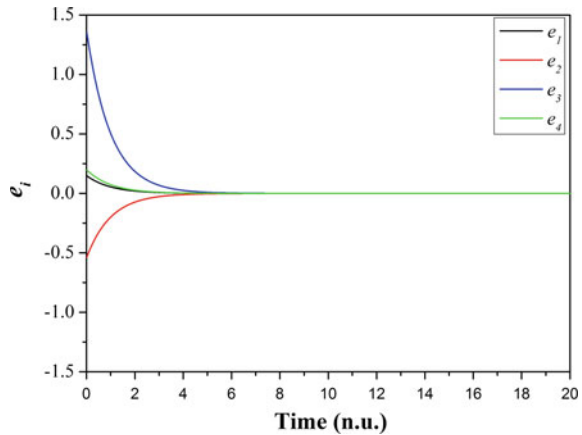


Fig. 39 The plot of errors $e_i (= \beta y_i - \alpha x_i)$, for $\alpha = -\beta = -1$, $c = 2.7$ and $d = 0.44$



time-series of x_2, y_2 (Fig. 38). Also, the plot of errors $e_i = y_i + x_i$ in Fig. 39 confirms the anti-synchronization of the coupled system.

3.2.3 The Case $\alpha = 2, \beta = 1$

In this case, the parameters of the error functions are chosen as $\alpha = 2$ and $\beta = 1$. By choosing the systems' parameters as $c = 2.7, d = 0.44$ and for $\alpha = 2$ the chaotic attractor of the second system is enlarged by two times, as it is shown with red color in Fig. 40, as well as by the time-series of signals y_1 and y_2 in regard to the signals x_1 and x_2 respectively (Figs. 42 and 43). The y_1 versus x_1 plot in Fig. 41 confirms that the coupled system is in complete synchronization state independently of the values of the error's parameters α, β . The error plot $e_i = y_1 - 2x_1$ ($i = 1, 2, 3, 4$) in Fig. 44

Fig. 40 The phase portraits of x_2 versus x_1 and y_2 versus y_1 , for $\alpha = 2, \beta = 1, c = 2.7$ and $d = 0.44$

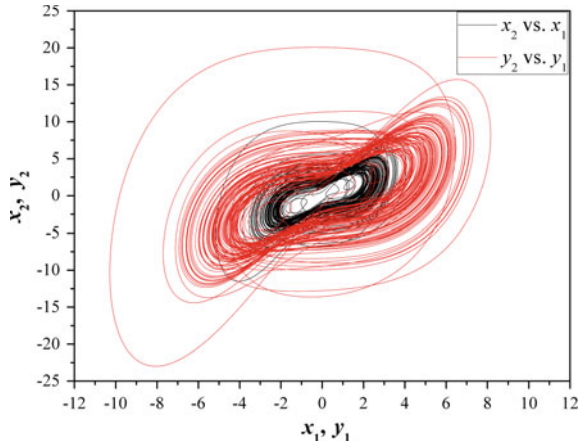


Fig. 41 The phase portrait of y_1 versus x_1 , for $\alpha = 2, \beta = 1, c = 2.7$ and $d = 0.44$

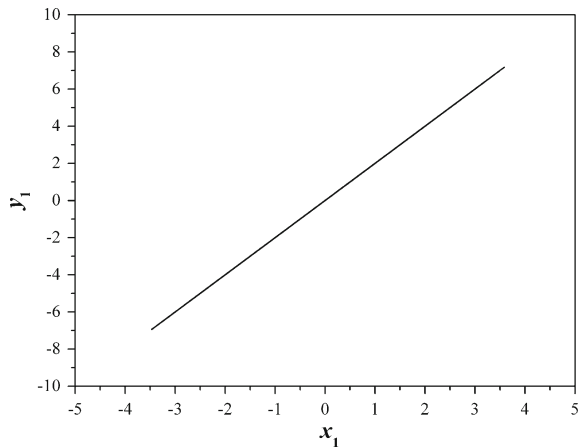


Fig. 42 The time-series of x_1, y_1 , for $\alpha = 2, \beta = 1, c = 2.7$ and $d = 0.44$

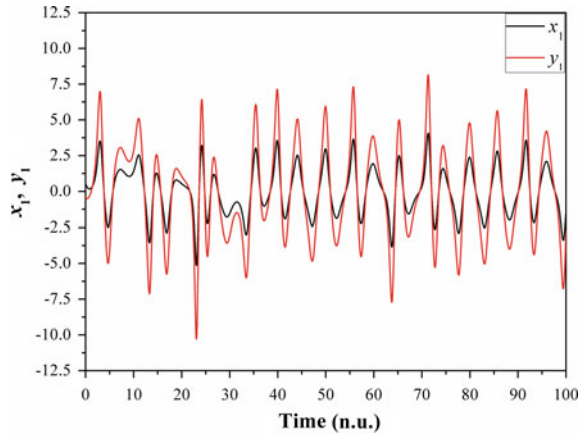


Fig. 43 The time-series of x_2, y_2 , for $\alpha = 2, \beta = 1, c = 2.7$ and $d = 0.44$

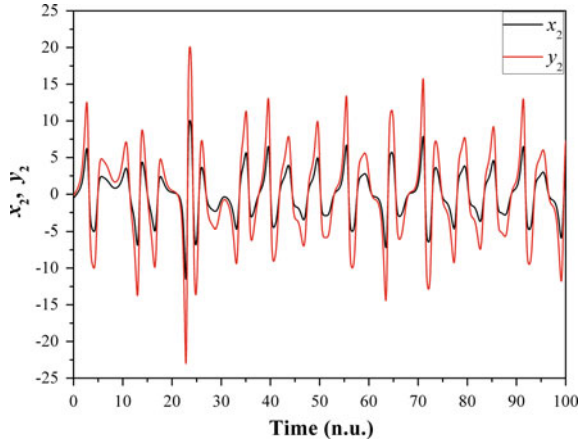
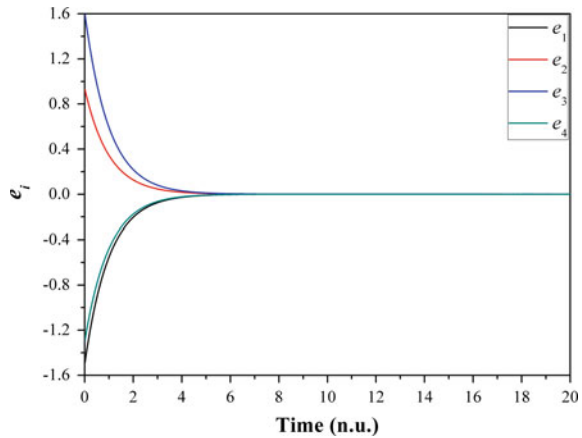


Fig. 44 The plot of errors $e_i (= \beta y_i - \alpha x_i)$, for $\alpha = 2, \beta = 1, c = 2.7$ and $d = 0.44$



shows the exponential convergence to zero that confirms the realization of system's complete synchronization state.

3.2.4 The Case $\alpha = -2, \beta = 1$

In the last case the parameters of the error function are chosen as $\alpha = -2$ and $\beta = 1$. So, the attractor of the first coupled system has been enlarged again by factor two, while the attractor of the second coupled system has been inverted in regard to the first one, as it is shown in Fig. 45. In this case the systems' parameters are chosen as $c = 2.7$ and $d = 0.44$ so as both of the coupled systems are in hyperchaotic state. This process is shown more clearly in the plots of the time series of x_1, y_1 and x_2, y_2 of Figs. 47 and 48. The phase portrait of y_1 versus x_1 in Fig. 46 indicates that the coupled system is in anti-synchronization state, which is also confirmed by the error plot $e_i = 2y_i + x_i$ ($i = 1, 2, 3, 4$) in Fig. 49.

Fig. 45 The phase portrait of x_2 versus x_1 , for $\alpha = -2$, $\beta = 1$, $c = 2.7$ and $d = 0.44$

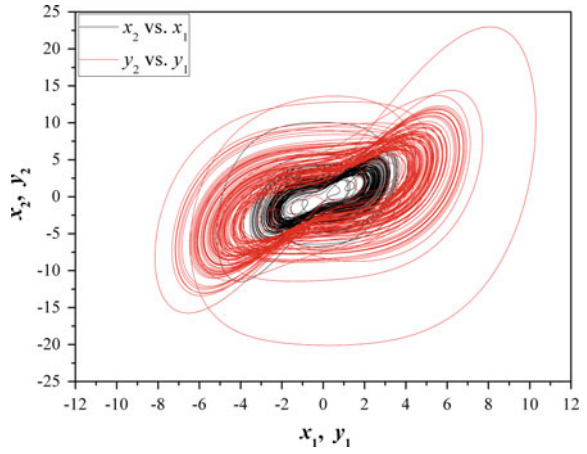


Fig. 46 The phase portrait of y_1 versus x_1 , for $\alpha = -2$, $\beta = 1$, $c = 2.7$ and $d = 0.44$

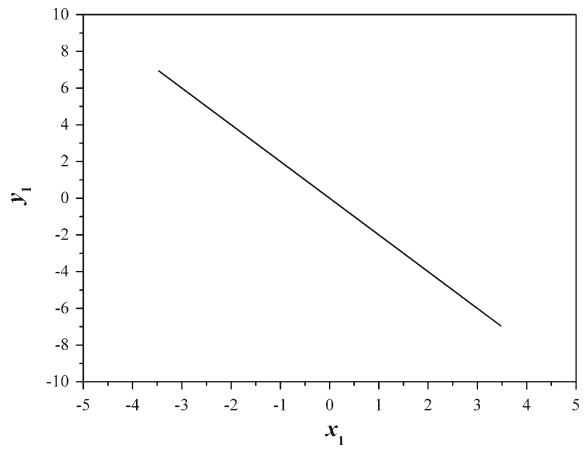


Fig. 47 The time-series of x_1, y_1 , for $\alpha = -2$, $\beta = 1$, $c = 2.7$ and $d = 0.44$

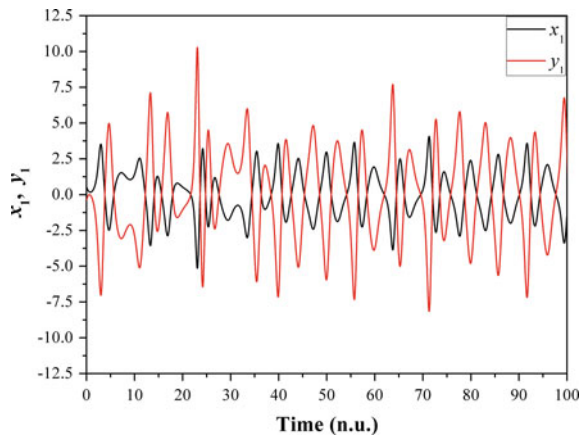


Fig. 48 The time-series of x_2, y_2 , for $\alpha = -2, \beta = 1, c = 2.7$ and $d = 0.44$

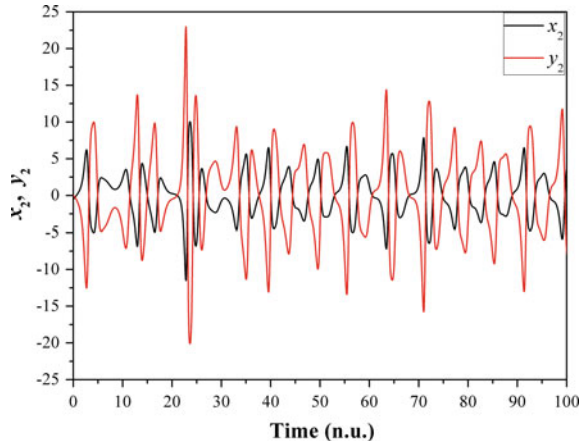
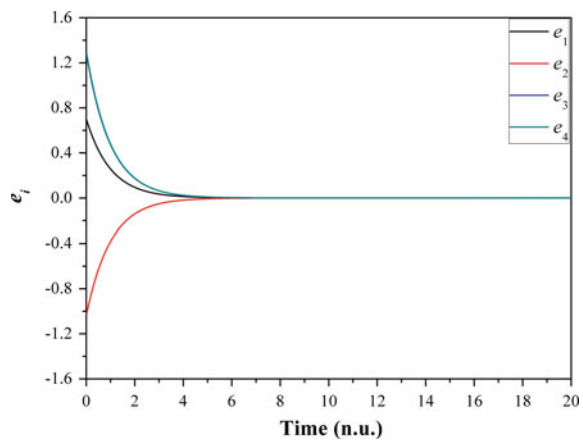


Fig. 49 The plot of errors $e_i (= \beta y_i - \alpha x_i)$, for $\alpha = -2, \beta = 1, c = 2.7$ and $d = 0.44$



4 Circuit’s Implementation of the Proposed Scheme

In this section the circuit implementation of the proposed scheme, with the electronic simulation package Cadence OrCAD, in the case of unidirectional coupling systems with $a = \beta$ is presented, in order to prove the feasibility of this method. The coupling system is realized by common electronic components. The system’s circuit consists of three sub-circuits, which are the master circuit, the slave circuit and the coupling circuit.

Figure 50 depicts the schematic of the master circuit. It has four integrators (U_1, U_2, U_3 and U_4) and two differential amplifiers (U_7, U_8), which are implemented with the TL084, as well as two signals multipliers (U_5, U_6) by using the AD633. By applying Kirchhoff’s circuit laws, the corresponding circuital equations of designed master circuit can be written as:

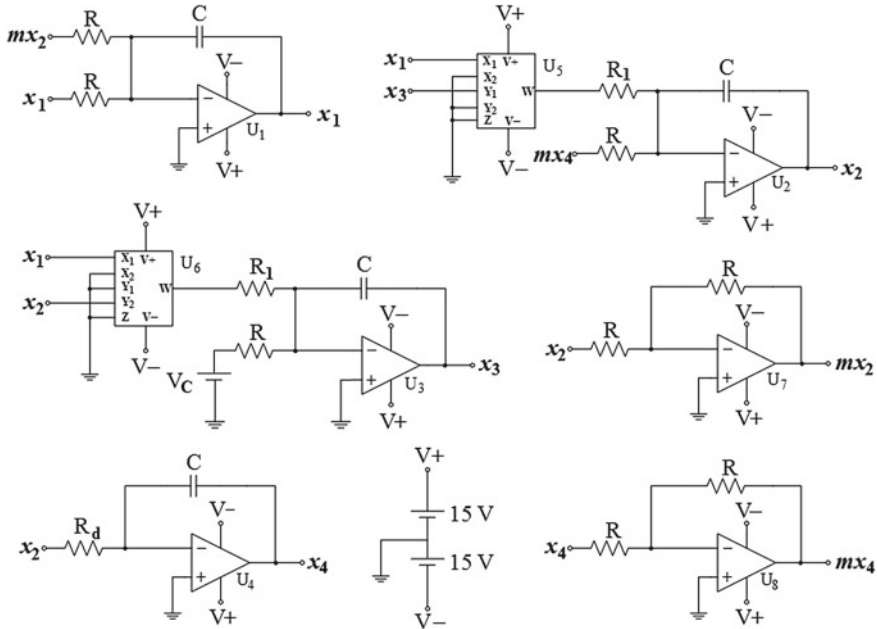


Fig. 50 The schematic of the master circuit

$$\begin{cases} \dot{x}_1 = \frac{1}{RC} (x_2 - x_1) \\ \dot{x}_2 = \frac{1}{RC} \left(-\frac{R}{R_1 10V} x_1 x_3 + x_4 \right) \\ \dot{x}_3 = \frac{1}{RC} \left(\frac{R}{R_1 10V} x_1 x_2 - c \right) \\ \dot{x}_4 = \frac{1}{RC} \left(-\frac{R}{R_d} x_2 \right) \end{cases} \quad (18)$$

where $x_i (i = 1, \dots, 4)$ are the voltages in the outputs of the operational amplifiers U_1, U_2, U_3 and U_4 . Normalizing the differential equations of system (18) by using $\tau = t/RC$ we could see that this system is equivalent to the system (12). The circuit components have been selected as: $R = 10\text{ k}\Omega$, $R_1 = 1\text{ k}\Omega$, $R_d = 22.727\text{ k}\Omega$, $C = 10\text{ nF}$, $V_c = 2.7\text{ V}$, while the power supplies of all active devices are $\pm 15\text{ V}_{DC}$. For the chosen set of components the master system's parameters are: $c = 2.7$ and $d = 0.44$. In Figs. 51, 52, 53, 54 and 55 the hyperchaotic attractors, which are obtained from Cadence OrCAD in various phase planes, are proved to be in a very good agreement with the respective phase portraits from system's simulation process (Figs. 15, 16, 17, 18 and 19). So, the proposed circuit emulates well the master system.

In Fig. 56 the schematic of the slave circuit, which is similar to the master circuit, is shown. The difference of this circuit in comparison to the previous one are the signals mu_2, mu_3 and mu_4 , which are the opposites of the signals U_{Y2}, U_{Y3} and U_{Y4} , produced by the controllers of Eq. (16). Also, e_2 is the difference signal $(\beta y_2 - \alpha x_2)$.

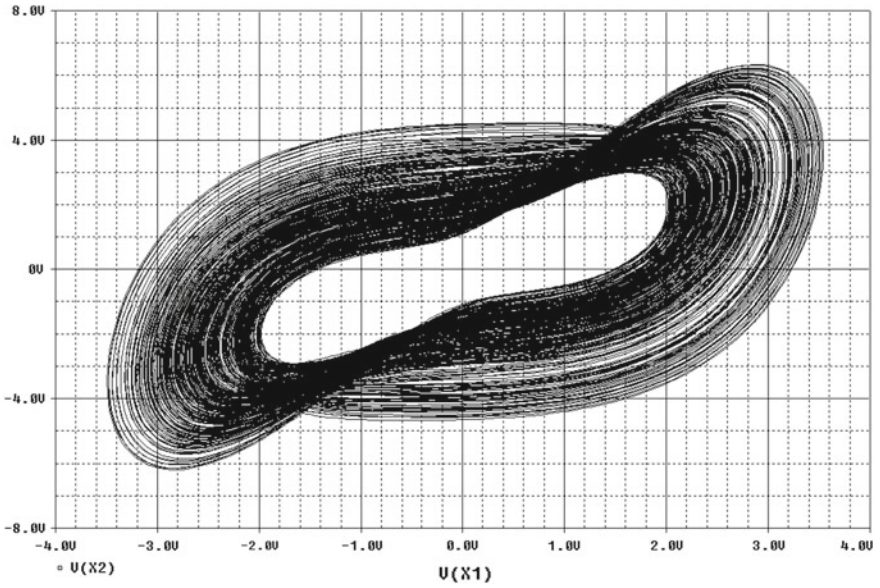


Fig. 51 Hyperchaotic attractor of the designed master circuit obtained from Cadence OrCAD in the (x_1, x_2) phase plane

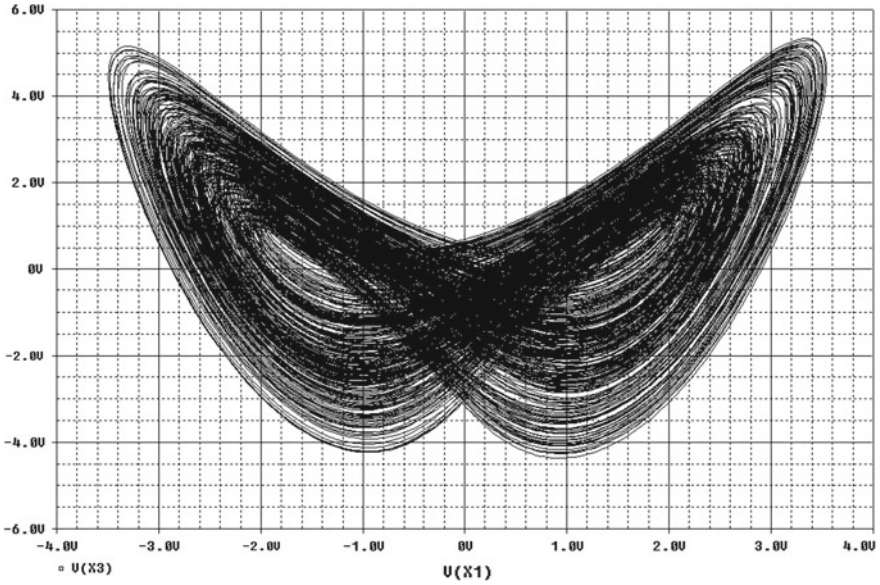


Fig. 52 Hyperchaotic attractor of the designed master circuit obtained from Cadence OrCAD in the (x_1, x_3) phase plane

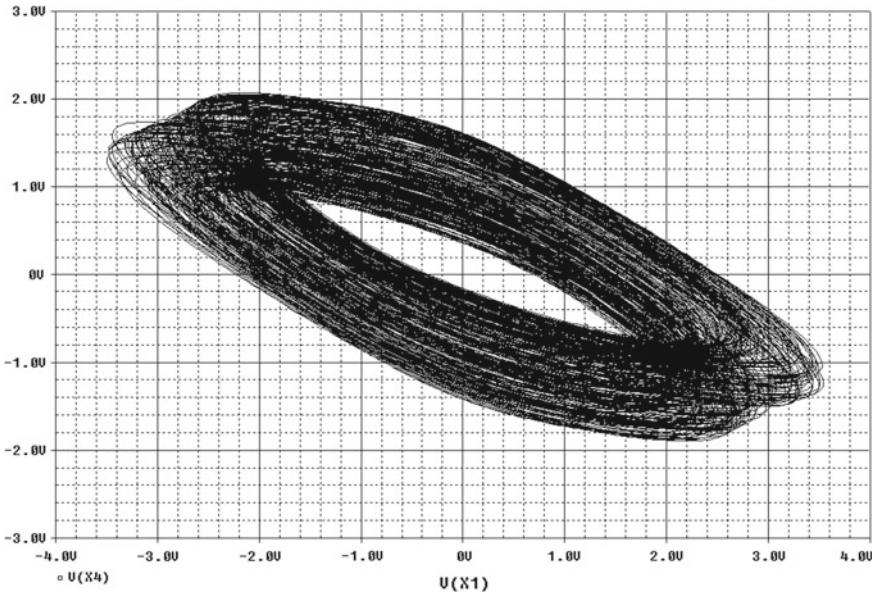


Fig. 53 Hyperchaotic attractor of the designed master circuit obtained from Cadence OrCAD in the (x_1, x_4) phase plane

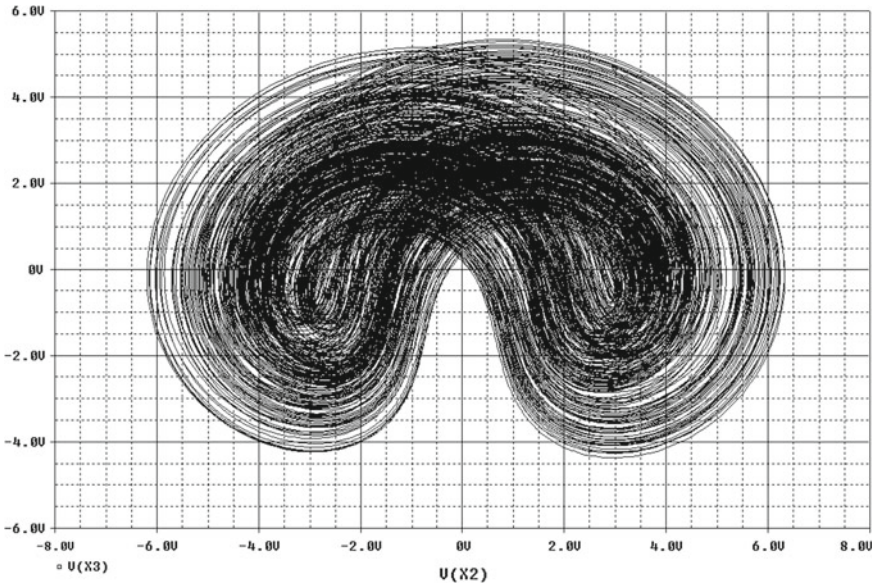


Fig. 54 Hyperchaotic attractor of the designed master circuit obtained from Cadence OrCAD in the (x_2, x_3) phase plane

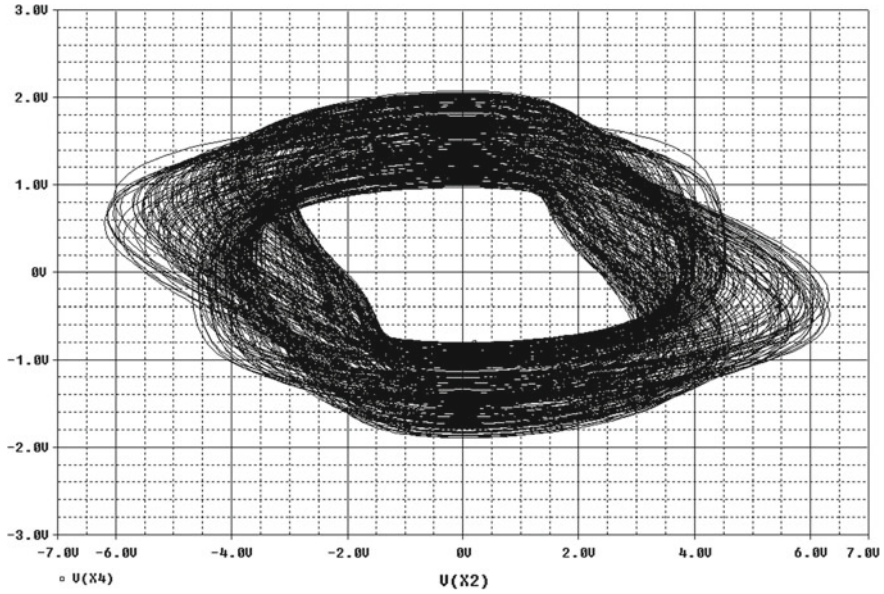


Fig. 55 Hyperchaotic attractor of the designed master circuit obtained from Cadence OrCAD in the (x_2, x_4) phase plane

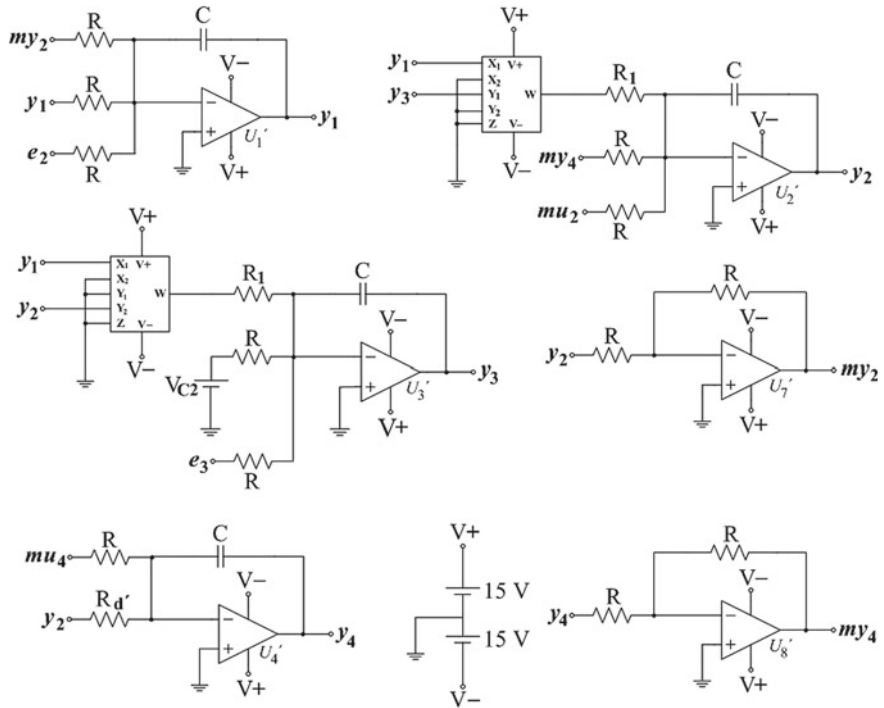


Fig. 56 The schematic of the slave circuit

Next, the design of the coupling circuit as well as the simulation results obtained from SPICE in the case of $\alpha = \beta$ is discussed in details.

In the case of $\alpha = \beta = 1$ and by considering the achievement of synchronization between the coupled systems (12) and (13), the NOLCs take the following forms.

$$\begin{cases} U_{Y1} = -e_2 \\ U_{Y2} = -(e_2 + e_4) \\ U_{Y3} = -e_3 \\ U_{Y4} = -(e_4 - de_2) \end{cases} \quad (19)$$

The units from which the coupling circuit is consisted, are shown in the schematic of Fig. 57. In this schematic u_2 and u_4 are the control signals U_{Y2} and U_{Y4} of Eq. (19)

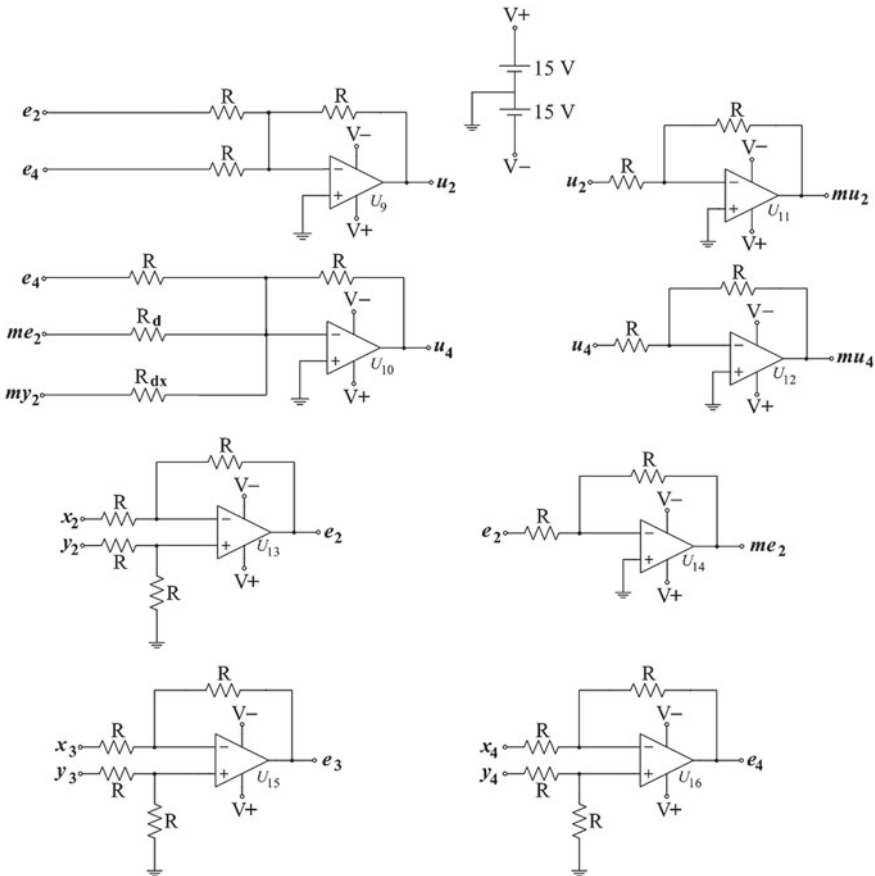


Fig. 57 The schematic of the coupling circuit

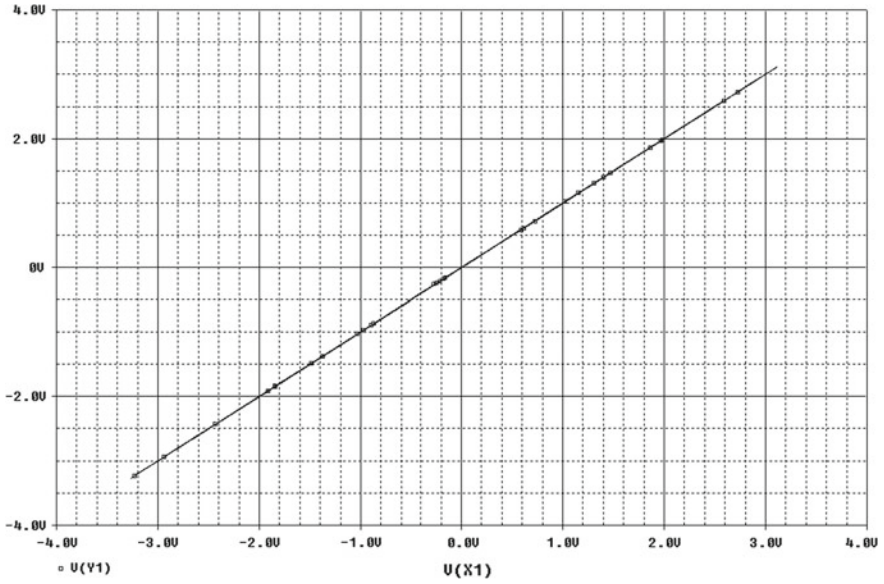


Fig. 58 The phase portrait in the (x_1, y_1) phase plane, for $\alpha = \beta = 1$, $c = 2.7$ and $d = 0.44$, obtained from Cadence OrCAD

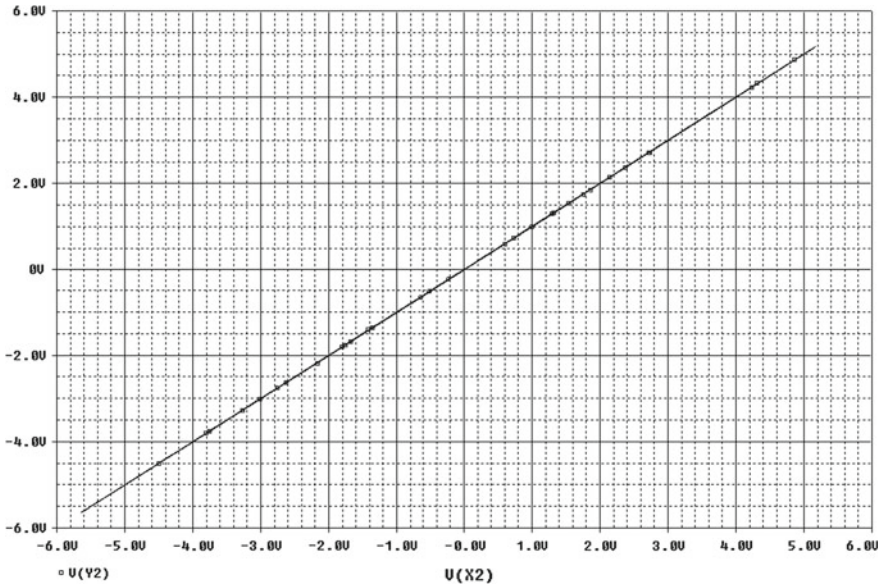


Fig. 59 The phase portrait in the (x_2, y_2) phase plane, for $\alpha = \beta = 1$, $c = 2.7$ and $d = 0.44$, obtained from Cadence OrCAD

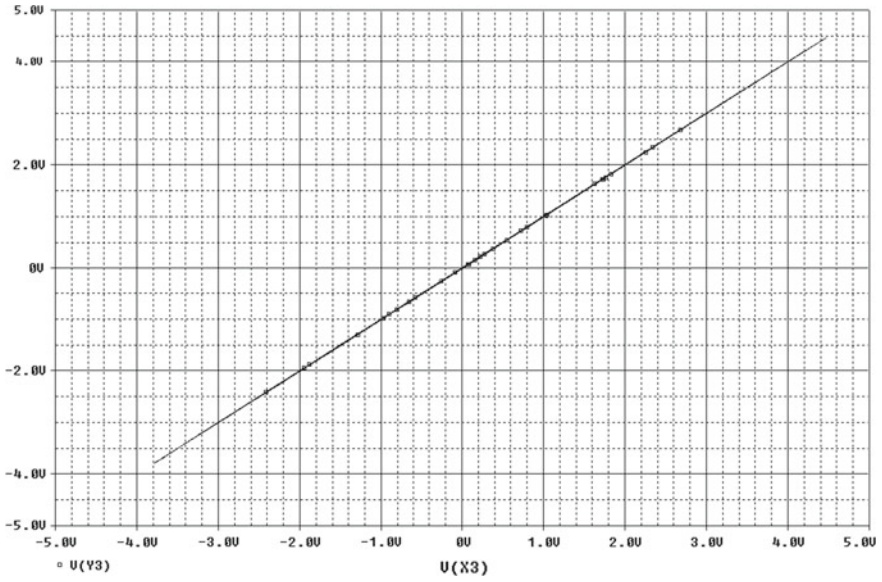


Fig. 60 The phase portrait in the (x_3, y_3) phase plane, for $\alpha = \beta = 1, c = 2.7$ and $d = 0.44$, obtained from Cadence OrCAD

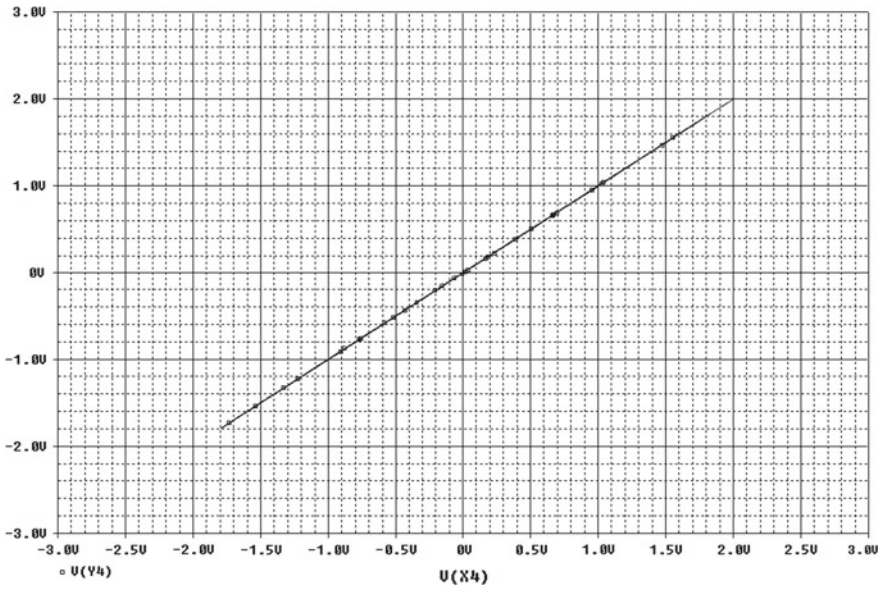


Fig. 61 The phase portrait in the (x_4, y_4) phase plane, for $\alpha = \beta = 1, c = 2.7$ and $d = 0.44$, obtained from Cadence OrCAD

respectively, while mu_2 and mu_4 are the opposite of these signals. Also, e_i , ($i = 2, 3, 4$) are the difference signals ($\beta y_i - \alpha x_i$, $i = 2, 3, 4$) and me_2 is the opposite of e_2 .

Figures 58, 59, 60 and 61 depict the phase portraits in (x_i, y_i) phase plane, with $i = 1, \dots, 4$, for $\alpha = \beta = 1$, $c = 2.7$ and $d = 0.44$, obtained from Cadence OrCAD. These figures confirm the achievement of complete synchronization in the case of unidirectionally coupled circuits with the proposed method.

5 Conclusion

In this chapter, the case of bidirectional and unidirectional coupling scheme of hyperchaotic dynamical systems with hidden attractors was studied. The proposed system is a four-dimensional modified Lorenz system, which is the simplest hyperchaotic system of this family. Furthermore, the coupling method was based on a recently new proposed scheme based on the nonlinear open loop controller.

According to the simulation results from system's numerical integration as well as the circuitual implementation of the proposed system in SPICE, in the case of unidirectional coupling, the appearance of complete synchronization and anti-synchronization, depending on the signs of the parameters of the error functions, was investigated in various cases. So, by choosing an appropriate sign for the error functions one could drive the coupling system either in complete synchronization or anti-synchronization behavior.

As it is known, the complex behavior of hyperchaotic systems, like the aforementioned, makes the control difficult in practical applications where a particular dynamic is desired. So, this chapter presents an interesting research result for the family of hyperchaotic systems with hidden attractors, because this method could be very useful in many potential applications of these systems. As a next step in this direction is the application of the proposed method in non-identical coupling systems in order to satisfy the goal of control of systems, which are in totally different dynamical behaviors.

References

1. Astakhov V, Shabunin A, Anishchenko V (2000) Antiphase synchronization in symmetrically coupled self-oscillators. *Int J Bifurc Chaos* 10:849–857
2. Bautin NN (1939) On the number of limit cycles generated on varying the coefficients from a focus or centre type equilibrium state. *Doklady Akademii Nauk SSSR* 24:668–671
3. Bautin NN (1952) On the number of limit cycles appearing on varying the coefficients from a focus or centre type of equilibrium state. *Mat Sb (N.S.)* 30:181–196
4. Bernat J, Llibre J (1996) Counterexample to Kalman and Markus-Yamabe conjectures in dimension larger than 3. *Dyn Contin Discret Impul Syst* 2:337–379
5. Blazejczuk-Okolewska B, Brindley J, Czolczynski K, Kapitaniak T (2001) Antiphase synchronization of chaos by noncontinuous coupling: two impacting oscillators. *Chaos Solitons Fract* 12:1823–1826

6. Cao LY, Lai YC (1998) Antiphase synchronism in chaotic system. *Phys Rev* 58:382–386
7. Dimitriev AS, Kletsovi AV, Laktushkin AM, Panas AI, Starkov SO (2006) Ultrawide-band wireless communications based on dynamic chaos. *J Commun Technol Electron* 51: 1126–1140
8. Dykman GI, Landa PS, Neymark YI (1991) Synchronizing the chaotic oscillations by external force. *Chaos Solitons Fract* 1:339–353
9. Enjieu Kadji HG, Chabi Orou JB, Woafu P (2008) Synchronization dynamics in a ring of four mutually coupled biological systems. *Commun Nonlinear Sci Numer Simul* 13:1361–1372
10. Fitts RE (1966) Two counterexamples to Aizerman's conjecture. *Trans IEEE AC-11*:553–556
11. Fujisaka H, Yamada T (1983) Stability theory of synchronized motion in coupled-oscillator systems. *Prog Theor Phys* 69:32–47
12. Gao Z, Zhang C (2011) A novel hyperchaotic system. *J Jishou Univ (Natural Science Edition)* 32:65–68
13. Gonzalez-Miranda JM (2004) Synchronization and control of chaos. Imperial College Press, London
14. Grassi G, Mascolo S (1999) Synchronization of high-order oscillators by observer design with application to hyperchaos-based cryptography. *Int J Circ Theor Appl* 27:543–553
15. Gubar' NA (1961) Investigation of a piecewise linear dynamical system with three parameters. *J Appl Math Mech* 25:1011–1023
16. Hilbert D (1901) Mathematical problems. *Bull Am Math Soc* 8:437–479
17. Holstein-Rathlou NH, Yip KP, Sosnovtseva OV, Mosekilde E (2001) Synchronization phenomena in nephron-nephron interaction. *Chaos* 11:417–426
18. Jafari S, Sprott J (2013) Simple chaotic flows with a line equilibrium. *Chaos Solit Fract* 57:79–84
19. Jafari S, Haeri M, Tavazoei MS (2010) Experimental study of a chaos-based communication system in the presence of unknown transmission delay. *Int J Circ Theor Appl* 38:1013–1025
20. Kalman RE (1957) Physical and mathematical mechanisms of instability in nonlinear automatic control systems. *Trans ASME* 79:553–566
21. Kapranov M (1956) Locking band for phase-locked loop. *Radiofizika* 2:37–52
22. Kim CM, Rim S, Kye WH, Rye JW, Park YJ (2003) Anti-synchronization of chaotic oscillators. *Phys Lett A* 320:39–46
23. Kuznetsov NV, Leonov GA, Vagitsev VI (2010) Analytical-numerical method for attractor localization of generalized Chua's system. *IFAC Proc Vol (IFAC-PapersOnline)* 4(1):29–33
24. Kyprianidis IM, Stouboulos IN (2003) Synchronization of two resistively coupled nonautonomous and hyperchaotic oscillators. *Chaos Solitons Fract* 17:317–325
25. Kyprianidis IM, Stouboulos IN (2003) Chaotic synchronization of three coupled oscillators with ring connection. *Chaos Solitons Fract* 17:327–336
26. Kyprianidis IM, Volos ChK, Stouboulos IN, Hadjidemetriou J (2006) Dynamics of two resistively coupled Duffing-type electrical oscillators. *Int J Bifurc Chaos* 16:1765–1775
27. Kyprianidis IM, Bogiatzi AN, Papadopoulou M, Stouboulos IN, Bogiatzis GN, Bountis T (2006) Synchronizing chaotic attractors of Chua's canonical circuit. The case of uncertainty in chaos synchronization. *Int J Bifurc Chaos* 16:1961–1976
28. Kyprianidis IM, Volos ChK, Stouboulos IN (2008) Experimental synchronization of two resistively coupled Duffing-type circuits. *Nonlinear Phenom Complex Syst* 11:187–192
29. Lauvdal T, Murray R, Fossen T (1997) Stabilization of integrator chains in the presence of magnitude and rate saturations: a gain scheduling approach. *IEEE Control Decision Conf*, pp 4004–4005
30. Leonov G, Kuznetsov NV (2013) Analytical-numerical methods for hidden attractors' localization: the 16th Hilbert problem, Aizerman and Kalman conjectures, and Chua circuits. *Numerical methods for differential equations, optimization, and technological problems, computational methods in applied sciences*. Springer 27:41–64
31. Leonov G, Kuznetsov N, Vagitsev V (2011) Localization of hidden Chua's attractors. *Phys Lett A* 375:2230–2233

32. Leonov G, Kuznetsov N, Kuznetsova O, Seldedzhi S, Vagitsev V (2011) Hidden oscillations in dynamical systems. *Trans Syst Contr* 6:54–67
33. Leonov G, Kuznetsov N, Vagitsev V (2012) Hidden attractor in smooth Chua system. *Physica D* 241:1482–1486
34. Li GH (2009) Inverse lag synchronization in chaotic systems. *Chaos Solitons Fract* 40: 1076–1080
35. Li C, Sprott JC (2014) Coexisting hidden attractors in a 4-D simplified Lorenz system. *Int J Bifurc Chaos* 24(3):1450034
36. Liu W, Qian X, Yang J, Xiao J (2006) Antisynchronization in coupled chaotic oscillators. *Phys Lett A* 354:119–125
37. Liu X, Chen T (2010) Synchronization of identical neural networks and other systems with an adaptive coupling strength. *Int J Circ Theor Appl* 38:631–648
38. Mainieri R, Rehacek J (1999) Projective synchronization in three-dimensional chaotic system. *Phys Rev Lett* 82:3042–3045
39. Maritan A, Banavar J (1994) Chaos noise and synchronization. *Phys Rev Lett* 72:1451–1454
40. Markus L, Yamabe H (1960) Global stability criteria for differential systems. *Osaka Math J* 12:305–317
41. Mosekilde E, Maistrenko Y, Postnov D (2002) *Chaotic synchronization: applications to living systems*. World Scientific, Singapore
42. Munmuangsaen B, Srisuchinwong B (2009) A new five-term simple chaotic attractor. *Phys Lett A* 373:4038–4043
43. Paar V, Pavin N (1998) Intermingled fractal Arnold tongues. *Phys Rev E* 57:1544–1549
44. Padmanaban E, Hens C, Dana K (2011) Engineering synchronization of chaotic oscillator using controller based coupling design. *Chaos* 21:013110
45. Parlitz U, Junge L, Lauterborn W, Kocarev L (1996) Experimental observation of phase synchronization. *Phys Rev E* 54:2115–2217
46. Pham V-T, Volos ChK, Jafari S, Wang X, Vaidyanathan S (2014) Hidden hyperchaotic attractor in a novel simple memristive neural network. *J Optoelectron Adv Mater Rapid Commun* 8(11–12):1157–1163
47. Pham V-T, Jafari S, Volos ChK, Wang X, Golpayegani Mohammad Reza Hashemi S (2014) Is that really hidden? The presence of complex fixed-points in chaotic flows with no equilibria. *Int J Bifurc Chaos* 24(11):1450146
48. Pecora LM, Carroll TL (1990) Synchronization in chaotic systems. *Phys Rev Lett* 64:821–824
49. Pikovsky AS (1984) On the interaction of strange attractors. *Z Phys B—Condensed Matter* 55:149–154
50. Pikovsky AS, Maistrenko YL (2003) *Synchronization: theory and application*. Springer, Netherlands
51. Pikovsky AS, Rosenblum M, Kurths J (2003) *Synchronization: a universal concept in nonlinear sciences*. Cambridge University Press, Cambridge
52. Rosenblum MG, Pikovsky AS, Kurths J (1997) From phase to lag synchronization in coupled chaotic oscillators. *Phys Rev Lett* 78:4193–4196
53. Rulkov NF, Sushchik MM, Tsimring LS, Abarbanel HDI (1995) Generalized synchronization of chaos in directionally coupled chaotic systems. *Phys Rev E* 51:980–994
54. Szatmári I, Chua LO (2008) Awakening dynamics via passive coupling and synchronization mechanism in oscillatory cellular neural/nonlinear networks. *Int J Circ Theor Appl* 36:525–553
55. Tafo Wembe E, Yamapi R (2009) Chaos synchronization of resistively coupled Duffing systems: numerical and experimental investigations. *Commun Nonlinear Sci Numer Simul* 14: 1439–1453
56. Taherion S, Lai YC (1999) Observability of lag synchronization of coupled chaotic oscillators. *Phys Rev E* 59:R6247–R6250
57. Tognoli E, Kelso JAS (2009) Brain coordination dynamics: true and false faces of phase synchrony and metastability. *Prog Neurobiol* 87:31–40
58. Tsuji S, Ueta T, Kawakami H (2007) Bifurcation analysis of current coupled BVP oscillators. *Int J Bifurc Chaos* 17:837–850

59. Van der Schrier G, Maas LRM (2000) The diffusionless Lorenz equations: Shil'nikov bifurcations and reduction to an explicit map. *Phys Nonlinear Phenom* 141:19–36
60. Volos ChK, Kyprianidis IM, Stouboulos IN (2006) Experimental demonstration of a chaotic cryptographic scheme. *WSEAS Trans Circ Syst* 5:1654–1661
61. Voss HU (2000) Anticipating chaotic synchronization. *Phys Rev E* 61:5115–5119
62. Wang J, Che YQ, Zhou SS, Deng B (2009) Unidirectional synchronization of Hodgkin-Huxley neurons exposed to ELF electric field. *Chaos Solitons Fract* 39:1335–1345
63. Wofo P, Enjieu Kadji HG (2004) Synchronized states in a ring of mutually coupled self-sustained electrical oscillators. *Phys Rev E* 69:046206
64. Zhong GQ, Man KF, Ko KT (2001) Uncertainty in chaos synchronization. *Int J Bifurc Chaos* 11:1723–1735